Journal of Theoretical Biology 301 (2012) 67–82

Contents lists available at SciVerse ScienceDirect

Journal of Theoretical Biology

journal homepage: www.elsevier.com/locate/yjtbi

A multiscale approach to curvature modulated sorting in biological membranes

M. Mercker [a,*], M. Ptashnyk [b,d], J. Kühnle [a], D. Hartmann [a], M. Weiss [c], W. Jäger [a]

[a] BioQuant, Im Neuenheimer Feld 267, D-69120 Heidelberg, Germany
[b] RWTH Aachen University, Department of Mathematics I, D-52056 Aachen, Germany
[c] University Bayreuth, Lehrstuhl Experimentalphysik I, D-95447 Bayreuth, Germany
[d] University of Dundee, Division of Mathematics, Dundee DD1 5EH, Scotland, UK

ARTICLE INFO

Article history:
Received 15 March 2011
Received in revised form
26 January 2012
Accepted 27 January 2012
Available online 9 February 2012

Keywords:
Phase separation
Gaussian rigidity
Lipid bilayer
Molecular dynamics
Upscaling

ABSTRACT

Combining different theoretical approaches, curvature modulated sorting in lipid bilayers fixed on non-planar surfaces is investigated. First, we present a continuous model of lateral membrane dynamics, described by a nonlinear PDE of fourth order. We then prove the existence and uniqueness of solutions of the presented model and simulate membrane dynamics using a finite element approach. Adopting a truly multiscale approach, we use dissipative particle dynamics (DPD) to parameterize the continuous model, i.e. to derive a corresponding macroscopic model.

Our model predicts that curvature modulated sorting can occur if lipids or proteins differ in at least one of their macroscopic elastic moduli. Gradients in the spontaneous curvature, the bending rigidity or the Gaussian rigidity create characteristic (metastable) curvature dependent patterns. The structure and dynamics of these membrane patterns are investigated qualitatively and quantitatively using simulations. These show that the decomposition time decreases and the stability of patterns increases with enlarging moduli differences or curvature gradients. Presented phase diagrams allow to estimate if and how stable curvature modulated sorting will occur for a given geometry and set of elastic parameters. In addition, we find that the use of upscaled models is imperative studying membrane dynamics. Compared with common linear approximations the system can evolve to different (meta)stable patterns. This emphasizes the importance of parameters and realistic dynamics in mathematical modeling of biological membranes.

1. Introduction

Biological membranes define a mechanical boundary of cells and of substructures inside cells. They provide environments specialized for certain chemical or mechanical processes. The main component of membranes is lipid molecules. In water lipids form, due to hydrophobic interactions, a bilayer structure consisting of two lipid monolayers physically opposed to each other. Since membrane molecules can move freely in lateral direction of the membrane, its lateral behavior can be compared to a two-dimensional (2D) fluid, first described in the 'fluid mosaic' model by Singer and Nicolson (1972). With respect to bending the membrane behaves elastically and in the linear regime is well described by the plate equation (Ciarlet, 1997).

In vivo, biological membranes are composed of many different lipids, proteins and other molecules with different functions (Alberts et al., 2006). Lateral sorting of these components is essential for maintaining the diversity of different membrane systems inside the cell as well as their function (Gennis, 1989). For both, lipids (Baumgart et al., 2003) and proteins (Bonifacino and Lippincott-Schwartz, 2003) lateral phase separation and clustering have been shown. It is widely accepted that membrane curvature modulated sorting is a basal mechanism controlling the spatial organization of lipids and proteins in the absence of specific chemical interactions. However, the exact underlying mechanisms remain mostly unknown (Tian and Baumgart, 2009).

Different membrane model systems, whose geometry, size and composition can be modified in a defined way, have been used to investigate curvature dependent sorting on different scales, experimentally as well as theoretically: experiments with artificial membranes have been performed using unilamellar vesicles (Baumgart et al., 2003; Heinrich et al., 2010; Kamal et al., 2009; Pencer et al., 2008; Roux et al., 2005; Tian and Baumgart, 2009) as well as solid supported membranes (Parthasarathy et al., 2006; Yoon et al., 2006). On the theoretical side, molecular dynamical approaches have been used to investigate the impact of molecular

* Corresponding author. Tel.: +49 6221 54 51336; mobile: +49 163 2357602.
E-mail address: mmercker_bioscience@gmx.de (M. Mercker).

0022-5193/$ - see front matter © 2012 Elsevier Ltd. All rights reserved.
doi:10.1016/j.jtbi.2012.01.039

parameters (Cooke and Deserno, 2006; Risselada and Marrink, 2009). But these are limited to small spatial and temporal scales due to computational complexity of the corresponding models. To investigate upper scales and to compare experiments with analytical estimates different continuous approaches have been developed (Bozic et al., 2006; Derganc, 2007; Rózycki et al., 2008; Seifert, 1993; Mercker et al., 2011), mainly based on the minimization of a free energy. A curvature dependent free energy of lateral homogeneous membranes has been early described by Helfrich (1973)

$$F_{\text{Helfrich}} = \int \frac{\kappa}{2}(H-H_0)^2\, d\omega + \int \kappa_G K\, d\omega, \tag{1}$$

where $d\omega$ depicts the surface measure, H the mean curvature and K the Gaussian curvature, both depending on the geometry of the membrane. If C_1 and C_2 are the two principal curvatures, H is defined as their sum and K as their product (see also Fig. 1). H_0,κ,κ_G are the elastic moduli, which are constant if the membrane is lateral homogeneous. H_0 is the spontaneous curvature and represents the preferred curvature in the relaxed state. It is non-zero e.g. if membrane molecules are wedge-shaped. κ and κ_G are the bending rigidity and the Gaussian rigidity (often referred to as the saddle-splay modulus), respectively. Both represent the stiffness of the membrane: in tubular structures (were K vanishes; cf. Fig. 1B) κ penalizes curvatures; in saddle structures (were H vanishes; cf. Fig. 1A) κ_G causes a penalty of curvatures. In general structures both moduli contribute to the energy penalty of curved membranes and most of the geometries appearing in biological membranes exhibit various intermediate structures of tubes, saddle structures and spheres (Fig. 1A–C).

Considering non-homogeneous membranes, it has been shown that gradients in elastic moduli can exhibit a driving force for lateral curvature modulated sorting. Membrane proteins are drawn to regions with curvature adapted to the protein shape (Ramaswamy et al., 2000) and lipids with small bending rigidity are sorted to highly curved membrane regions (Parthasarathy et al., 2006), thus that lateral reorganization reduces the membrane curvature energy. Although various theoretical and experimental studies have been performed to investigate lateral sorting due to gradients in spontaneous curvature (Bozic et al., 2006; Cooke and Deserno, 2006; Derganc, 2007; Kamal et al., 2009; Leibler, 1986; Liang and Ma, 2009; Ramaswamy et al., 2000; Risselada and Marrink, 2009; Seifert, 1993) and bending rigidity (Baumgart et al., 2003; Derganc, 2007; Parthasarathy et al., 2006; Roux et al., 2005; Rózycki et al., 2008), the impact of the elusive Gaussian rigidity on lateral sorting has not been investigated so far. However, experimental studies show that different membrane components can differ distinctly in their Gaussian rigidities (Semrau et al., 2008).

In this study, we investigate theoretically the impact of an inhomogeneous Gaussian rigidity on lateral sorting and compare it with sorting due to gradients in the bending rigidity and spontaneous curvature. Following the experimental approach of Parthasarathy et al. (2006) and Roux et al. (2005), we consider membranes attached to non-planar substrates. Thus by considering a geometrically fixed membrane the complexity is reduced facilitating the extraction of hypotheses to be checked by experimentalists. To do so, a continuous model of lateral membrane dynamics, based on the minimization of a free energy, is derived. Considering a gradient flow of the free energy, we obtain a model in terms of a nonlinear PDE of fourth order, related to the Cahn–Hilliard equation (Cahn and Hilliard, 1958) (cf. Elliott and Garcke, 1996; Elliott and Songmu, 1986 for analytical results). In the following, we show that unique solutions exist and approximate them using a finite element approach. Adopting a multiscale approach, parametrization of the continuous model from the molecular scale has been achieved via upscaling from dissipative particle dynamic (DPD) studies. On the basis of this multiscale modeling approach, simulations are performed comparing dynamics and (metastable) patterns of lateral sorting.

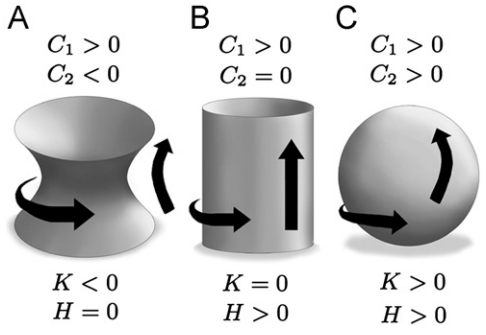

Fig. 1. Principle curvatures C_1,C_2, mean curvature $H=C_1+C_2$ and Gaussian curvature $K=C_1C_2$ for different geometries: (A) saddle, (B) tube, (C) sphere.

2. Theoretical model

2.1. Continuous approach

Following the ideas of Parthasarathy et al. (2006) and Roux et al. (2005), we consider a curved membrane represented by a fixed smooth Riemannian manifold Γ—in contrast to free membranes typically studied (Baumgart et al., 2003; Heinrich et al., 2010; Kamal et al., 2009; Pencer et al., 2008; Roux et al., 2005; Tian and Baumgart, 2009), where Γ itself is evolving in time. Here, we consider a membrane composed of two different molecule species, e.g. two different lipids or lipids and proteins. The concentration of the two components ϕ^A and ϕ^B in Γ is described by the order parameter $\phi : \Gamma \to [-1,1]$, where $\phi = \phi^A - \phi^B$. That is, if $\phi = 1$ the membrane is locally composed purely of species A and if $\phi = -1$ locally only species B is present.

It has been shown that sorting depends critically on membrane curvature and phase separation (in the absence of specific signals actively influencing lateral dynamics) (Parthasarathy et al., 2006; Roux et al., 2005). Therefore our model is based on the minimization of a free energy $F = F_1 + F_2$ containing both a curvature depending energy F_1 (related to Helfrich, 1973) and a Cahn–Hilliard energy F_2 (Cahn and Hilliard, 1958) modeling lateral phase separation. In detail, both parts read

$$\begin{aligned} F_1 &= \frac{1}{2}\int_\Gamma \kappa(\phi)(H-H_0(\phi))^2\, d\omega + \int_\Gamma \kappa_G(\phi) K\, d\omega, \\ F_2 &= \tilde{\sigma}\int_\Gamma \left(\frac{\xi^2}{2}(\nabla^\Gamma \phi)^2 + f(\phi)\right) d\omega. \end{aligned} \tag{2}$$

Describing the fact that different components may differ in their mechanical properties (such as shape and stiffness), each macroscopic elastic modulus h ($h \in \{\kappa,\kappa_G,H_0\}$) is taken as a function of the concentration ϕ. Each function h is chosen such that $h(1) = h^A$ and $h(-1) = h^B$, where h^A and h^B are the elastic moduli of the pure components. Furthermore, ξ is a transition length, $\sigma = \tilde{\sigma}\xi$ the line-tension, ∇^Γ the surface gradient and f a double well potential. The function $f : \mathbb{R} \to \mathbb{R}_+$ is of the form $f(\phi) = \frac{9}{32}(\phi^2-1)^2$. Instead of minimizing $F = F_1 + F_2$ directly we adopt a dynamic point of view. Thus assuming local mass conservation lateral dynamics of the two species A and B are determined by the lateral continuity equation

$$\partial_t \phi + \nabla^\Gamma \cdot \vec{j} = 0,$$

where $\nabla^\Gamma\cdot$ is the surface divergence operator. The flux is determined by the lateral gradient of the chemical potential μ, i.e. $\vec{j}=\nabla^\Gamma\mu$; the chemical potential μ is proportional to the variation of the free energy F with respect to ϕ, thus $\mu=L_\phi(\delta/\delta\phi)[F]$; the mobility L_ϕ is assumed to be constant (scaling inversely with the viscosity of the membrane—the corresponding diffusion coefficient is given by $D=L_\phi\tilde{\sigma}$). Altogether, we have the following evolution equation for ϕ:

$$\partial_t[\phi]=L_\phi\Delta^\Gamma\left[\frac{\delta}{\delta\phi}[F]\right]=L_\phi\Delta^\Gamma\left[\frac{1}{2}\kappa'(\phi)(H-H_0(\phi))^2 -\kappa(\phi)(H-H_0(\phi))H_0'(\phi)+\kappa_G'(\phi)K-\tilde{\sigma}(\xi^2\Delta^\Gamma\phi-f'(\phi))\right]. \tag{3}$$

2.2. Analytical treatment

Existence and uniqueness results for the Cahn–Hilliard equation defined in a bounded domain of $\mathbb{R}^n$, with $n\le 3$, have been proven in Elliott and Garcke (1996) and Elliott and Songmu (1986). In contrast to the classical Cahn–Hilliard equation, Eq. (3) is considered on an arbitrarily shaped hyper-surface and the curvature depending part of the free energy introduces additional nonlinear terms. Therefore, we first address the question of existence and uniqueness of solutions to ensure the validity of our results and corresponding deductions. The curvature depending nonlinear terms require additional steps in the proof of existence, especially in the proof of corresponding a priori estimates. The boundedness of $\nabla^\Gamma\phi$ in $L^2(0,T;L^\infty(\Gamma))$ is essential for the uniqueness result.

Let $\overline{\Gamma}$ be a smooth compact Riemannian manifold with a boundary and $\dim(\Gamma)\le 3$. In the considered biological applications we have $\dim(\Gamma)=2$, however the existence and uniqueness results hold also for three-dimensional smooth Riemannian manifolds. We consider on Γ Eq. (3) and rewrite it in the form

$$\partial_t\phi+L_\phi\tilde{\sigma}\xi^2(\Delta^\Gamma)^2\phi=L_\phi\Delta^\Gamma R(\phi,H,K)\quad\text{in } (0,T)\times\Gamma, \tag{4}$$

with initial and boundary conditions

$$\phi(0,x)=\phi_0(x)\quad\text{in }\Gamma, \tag{5}$$

$$\nabla^\Gamma(\tilde{\sigma}\xi^2\Delta^\Gamma\phi-R(\phi,H,K))\cdot\nu=0,\quad \nabla^\Gamma\phi\cdot\nu=0\quad\text{on } (0,T)\times\partial\Gamma, \tag{6}$$

where Δ^Γ is the Laplace–Beltrami operator, ν is the unit outward normal vector to $\partial\Gamma$, and

$$R(\phi,H,K)=\tfrac{1}{2}\kappa'(\phi)(H-H_0(\phi))^2-\kappa(\phi)(H-H_0(\phi))H_0'(\phi)+\kappa_G'(\phi)K+\tilde{\sigma}f'(\phi).$$

Assumption 1. We assume $f(\phi)=\frac{9}{32}(\phi^2-1)^2$ and κ, κ_G, $H_0\in C^3(\mathbb{R})$ with κ', κ'', κ''', H_0', H_0'', $H_0''':\mathbb{R}\to\mathbb{R}$ bounded, and

$$|\kappa(\eta)|\le c_1|\eta|+c_2,\quad |H_0(\eta)|\le c_1|\eta|+c_2,$$
$$|\kappa_G(\eta)|+|\kappa_G'(\eta)|\le c_1|\eta|^3+c_2,\quad |\kappa_G''(\eta)|\le c_1|\eta|^2+c_2,$$
$$|\kappa_G'''(\eta)|\le c_1|\eta|+c_2,$$

for some positive constants c_1, c_2. The smoothness and compactness of $\overline{\Gamma}$ imply that the mean curvature H and the Gaussian curvature K are smooth and bounded.

For the initial data we assume $\phi_0\in H^2(\Gamma)$.

Definition 2. A function $\phi\in L^2(0,T;H^2(\Gamma))\cap H^1(0,T;L^2(\Gamma))$, such that

$$\int_0^T\int_\Gamma(\partial_t\phi\nu+L_\phi\tilde{\sigma}\xi^2\Delta^\Gamma\phi\Delta^\Gamma\nu)\,d\omega\,dt +L_\phi\int_0^T\int_\Gamma\nabla^\Gamma R(\phi,H,K)\nabla^\Gamma\nu\,d\omega\,dt=0, \tag{7}$$

for all $\nu\in L^2(0,T;H^2(\Gamma))$ and $\phi\to\phi_0$ in $L^2(\Gamma)$ as $t\to 0$, is called a weak solution of the problem (4)–(6) .

Theorem 3. *Under the Assumption1 on the functions κ, H_0, κ_G, f and the initial data, there exists a unique weak solution of* (4)–(6).

The extensive theory of Sobolev spaces and elliptic equations on Riemannian manifolds, enables a direct generalization of the known existence results for the Cahn–Hilliard equation in a bounded domain of $\mathbb{R}^n$ to the problem posed on a smooth Riemannian manifold. However, the nonlinear curvature depending terms in Eq. (4) require new steps in the proof of the existence of a solution. A different approach is also used to show the uniqueness result. Here, we summarize only the main ideas of the proof and for more details we refer to Appendix A.

Main ideas of the proof. *Existence*: We show the existence of a weak solution using the Galerkin method (Evans, 1998). Let $\{w_i\}_{i\in\mathbb{N}}$ be an orthogonal basis of $H^2(\Gamma)$, an orthonormal basis in $L^2(\Gamma)$ and the functions w_i are smooth. We are looking for a function $\phi^k(t,x)=\sum_{i=1}^k\alpha_i^k(t)w_i(x)$ in the finite-dimensional subspace W_k of $H^2(\Gamma)$ spanned by $\{w_1,\dots,w_k\}$, such that

$$\int_\Gamma(\partial_t\phi^k\nu+L_\phi\tilde{\sigma}\xi^2\Delta^\Gamma\phi^k\Delta^\Gamma\nu)\,d\omega+L_\phi\int_\Gamma\nabla^\Gamma R(\phi^k,H,K)\nabla^\Gamma\nu\,d\omega=0, \tag{8}$$

for $\nu\in W_k$ and $\phi_0^k=\sum_{i=1}^k(\phi_0,w_i)_{L^2(\Gamma)}w_i$ with $\phi_0^k\to\phi_0$ in $H^2(\Gamma)$. Using the a priori estimates from Lemma 4, presented in Appendix A, we obtain the convergence of a subsequence of $\{\phi_k\}$ in the appropriate function spaces. Then passing in (8) to the limes as $k\to\infty$ we obtain the existence of a weak solution of the problem (4)–(6) . The detailed proof is presented in Appendix A.

Uniqueness: We assume there exist two solutions ϕ_1, ϕ_2 of the problem (4)–(6). Eq. (7) with the test function $\nu=\phi_1-\phi_2$ implies that $\phi_1-\phi_2$ satisfies the equality

$$\int_0^\tau\int_\Gamma\frac{1}{2}\partial_t|\phi_1-\phi_2|^2\,d\omega\,dt+\int_0^\tau\int_\Gamma L_\phi\tilde{\sigma}\xi^2|\Delta^\Gamma(\phi_1-\phi_2)|^2\,d\omega\,dt +L_\phi\int_0^\tau\int_\Gamma\nabla^\Gamma(R(\phi_1,H,K)-R(\phi_2,H,K))\nabla^\Gamma(\phi_1-\phi_2)\,d\omega\,dt=0. \tag{9}$$

The third term in (9) can be estimated by

$$\int_0^\tau\int_\Gamma(C_\delta|\phi_1-\phi_2|^2+\delta_2|\Delta^\Gamma(\phi_1-\phi_2)|^2)\,d\omega\,dt+\delta_1\sup_{(0,\tau)}\int_\Gamma|\phi_1-\phi_2|^2\,d\omega,$$

with $0<\delta_1\le\frac{1}{4}$ and $0<\delta_2\le L_\phi\tilde{\sigma}\xi^2/2$. For explicit estimation steps see Appendix A. Then, the integration by parts in the first term in (9) and the fact $\phi_1(0,x)=\phi_2(0,x)$ yield

$$\int_\Gamma|\phi_1-\phi_2|^2\,d\omega+L_\phi\tilde{\sigma}\xi^2\int_0^\tau\int_\Gamma|\Delta^\Gamma(\phi_1-\phi_2)|^2\,d\omega\,dt \le 2C_\delta\int_0^\tau\int_\Gamma|\phi_1-\phi_2|^2\,d\omega\,dt+2\delta_1\sup_{(0,\tau)}\int_\Gamma|\phi_1-\phi_2|^2\,d\omega.$$

Using Gronwall inequality we obtain

$$\int_\Gamma|\phi_1(\tau,x)-\phi_2(\tau,x)|^2\,d\omega\le 2\delta_1\exp(2C_\delta\tau)\sup_{t\in(0,\tau)}\int_\Gamma|\phi_1(t,x)-\phi_2(t,x)|^2\,d\omega.$$

Then, there exists a τ such that $2\delta_1\exp(2C_\delta\tau)<1$ and

$$\sup_{(0,\tau)}\int_\Gamma|\phi_1-\phi_2|^2\,d\omega\le 0.$$

Thus, $\phi_1(t,x)=\phi_2(t,x)$ a.e. in $(0,\tau)\times\Gamma$ were τ is independent of ϕ_1 and ϕ_2. The iteration argument implies the uniqueness in $(0,T)\times\Gamma$, since τ can be chosen the same in each iteration step. □

Remark 2.1. Existence and uniqueness proofs for the periodic boundary conditions follows along the same lines.

2.3. Dissipative particle dynamics

Dissipative particle dynamics (DPD) is a versatile computer simulation technique that is particularly well suited for studying the behavior of lipid membranes on mesoscopic scales. Indeed, DPD has been employed to study various membrane-related processes such as lipid phase separation (Kranenburg et al., 2003; Laradji and Kumar, 2005, 2004), self-assembly of lipid vesicles (Yamamoto et al., 2002) and vesicle budding (Yamamoto, 2003). We outline the setup of a DPD simulation only briefly and refer the reader to Nikunen et al. (2003) for more technical details.

In DPD, atoms or groups of atoms are represented by spherical beads with mass m_i. Any two beads i,j with a distance $r_{ij}=|\mathbf{r}_{ij}|=|\mathbf{r}_i-\mathbf{r}_j|\le r_0$ are subject to a linear repulsive force $\mathbf{F}_{ij}^C=a_{ij}(1-r_{ij}/r_0)\mathbf{e}_{ij}$. The degree of hydrophobicity can be tuned via the interaction energies a_{ij}. Here $\mathbf{e}_{ij}=\mathbf{r}_{ij}/r_{ij}$ denotes the unit vector. Lipids are modeled as linear chains of a single hydrophilic head bead and three hydrophobic tail beads that are connected via a harmonic potential $U(\mathbf{r}_i,\mathbf{r}_{i+1})=k(r_{i,i+1}-l_0)^2/2$. The relaxation distance between two beads in the lipid is hence l_0. To impose an intrinsic stiffness to the lipid chains, a bending potential $V_b(\mathbf{r}_{i-1},\mathbf{r}_i,\mathbf{r}_{i+1})=k_{\text{bend}}(1-\cos(\Phi))$ is introduced between consecutive beads $i-1,i,i+1$. Here, $\cos(\Phi)=\mathbf{e}_{i,i-1}\mathbf{e}_{i,i+1}$, i.e. lipids try to assume the shape of a rigid rod.

DPD simulations are based on the above conservative forces combined with a DPD thermostat. The thermostat consists of a dissipative force $\mathbf{F}_i^Dj=-\gamma_{ij}(1-r_{ij}/r_0)^2(\mathbf{e}_{ij}\cdot\mathbf{v}_{ij})\mathbf{e}_{ij}$ and a random force $\mathbf{F}_i^Rj=\sigma_{ij}(1-r_{ij}/r_0)\xi_{ij}\mathbf{e}_{ij}$ for particles with $r_{ij}\le r_0$. Here, $\mathbf{v}_{ij}=\mathbf{v}_i-\mathbf{v}_j$ denotes the relative velocity between particle i and j and ξ_{ij} defines an uncorrelated random variable with vanishing mean and unit variance. The thermostat parameters are related via the fluctuation-dissipation theorem $\sigma_{ij}^2=2\gamma_{ij}k_BT$.

Following the approach of Schmidt et al. (2008), the interaction cutoff r_0, together with all bead masses and the thermostat temperature are set to unity. Comparable to Laradji and Kumar (2004) parameters are chosen as $\sigma_{ij}=3$, $\gamma_{ij}=9/2$, $k=100k_BT/r_0^2$, $l_0=0.45r_0$, $a_{HT}=a_{WT}=200k_BT$, whereas $a_{WW}=a_{HH}=a_{TT}=a_{WH}=25k_BT$. Here, W, H, T refer to water, lipid head and lipid tail beads, respectively. Lipids are represented as linear chains HT_3. Two types of lipids that differ in the bending rigidity of their chains ($\kappa_A^{DPD}=10k_BT$ and $\kappa_B^{DPD}=30k_BT$) are considered. Integration of the equations of motion is achieved using a velocity Verlet scheme with time increment $\Delta t=0.01$ and periodic boundary conditions. Membrane patches of the size $25r_0\times 25r_0$ are relaxed via a barostat (Jakobsen, 2005) for a period of 2×10^5 time steps. After this period, the membrane is in a tensionless state and fluctuations are recorded for 10^6 time steps with the size of the simulation box being held constant. Intrinsic DPD units can be converted to SI units by comparison of the typical membrane thickness to experimental values, yielding $r_0\approx 1$ nm.

2.4. Finite element approximation

The bilayer is represented by a continuous two-dimensional (2D) surface Γ depicted by a parametric representation $\vec{X}(u_1,u_2): U\to\Gamma\subset\mathbb{R}^3$, where $U=[0,1]\times[0,1]$, corresponding to a membrane patch of 12 μm × 12 μm. By means of numerical studies Eq. (3) will be investigated in detail using the finite element library Gascoigne (Becker et al., 2012). Since here only first-order derivatives are available, we discretize this fourth order PDE in a mixed formulation (Brezzi and Fortin, 1991), with bilinear finite elements.

Here, we shortly recapitulate the numerical approach adopted. Let us assume $0=t_0<t_1<\cdots<t_{M-1}<t_M=T$ is a discretization of the time interval $[0,T]$ into time steps $\tau_m:=t_{m+1}-t_m$, which are possibly variable. Further let us assume Γ^q is a conforming quadrangulation approximating Γ, where $\Gamma^q=\bigcup_{j=1}^J\bar{\tilde{v}}_j$ and $\{\tilde{v}_j\}_{j=1}^J$ is a family of mutually disjoint open quadrangles. We define the finite element space of globally continuous, piecewise bilinear elements by $V(\Gamma^q):=\{\psi\in C(\Gamma^q,\mathbb{R}):\psi|_{\tilde{v}_j}\text{ is bilinear }\forall j=1,\dots J\}\subset H^1(\Gamma^q,\mathbb{R})$. For scalar and vector valued functions $f,g\in L^2$ we introduce the L^2 inner product $\langle .,.\rangle$ over Γ^q as $\langle f,g\rangle:=\int_{\Gamma^q}(f\cdot g)\,d\omega$, where $f\cdot g$ denotes the usual inner product for scalars and vectors. Approximations $\mathcal{H}$ of the mean curvature H, $\mathcal{K}$ of the Gaussian curvature K and of other geometrical quantities concerning Γ are defined following the ideas of Barrett et al. (2008).

To reformulate the fourth order PDE (3) in a weak formulation using only first-order derivatives, we follow the idea of Elliott et al. (1989) introducing an additional variable substituting the chemical potential. This leads to the following discrete approximation of Eq. (3): for $m\ge 0$, find $\phi^{m+1},Y^{m+1}\in V(\Gamma^q)$ such that

$$\left\langle\frac{\phi^{m+1}-\phi^m}{\tau_m},\psi\right\rangle=-L_\phi\langle\nabla^\Gamma[Y^{m+1}],\nabla^\Gamma[\psi]\rangle\quad\forall\psi\in V(\Gamma^q)\tag{10}$$

and

$$\begin{aligned}\langle Y^{m+1},\psi\rangle=&\left\langle\frac{\kappa'(\phi^m)}{2}(\mathcal{H}-H_0(\phi^m))^2,\psi\right\rangle+\tilde{\sigma}\xi^2\left\langle\nabla^\Gamma[\phi^{m+1}],\nabla^\Gamma[\psi]\right\rangle\\&-\langle\kappa(\phi^m)(\mathcal{H}-H_0(\phi^m))H_0'(\phi^m)+\kappa_G'(\phi^m)\mathcal{K}+\tilde{\sigma}f'(\phi^m),\psi\rangle\\&\forall\psi\in V(\Gamma^q)\end{aligned}\tag{11}$$

hold.

3. Results

3.1. Microscopic scale—dissipative particle dynamics

Previous DPD studies on binary lipid mixtures have focused mainly on phase separation phenomena (Kranenburg et al., 2003; Laradji and Kumar, 2004, 2005) or the influence of lipid length on membrane stiffness (Illya et al., 2006; Imparato et al., 2005). Here, we use DPD simulations to parameterize the relation between the membrane's bending rigidity κ and the average local composition ϕ that enters the macroscopic continuum model. To do so, we consider DPD membranes of varying composition for which we determine directly the bending rigidity via the fluctuation spectrum of the bilayer. Since the Gaussian bending rigidity κ_G cannot be measured directly (Siegel and Kozlov, 2004), we restrict the analysis to the bending rigidity κ. Indeed, for the chosen parameter set, the two lipid species form a well-mixed, tensionless homogeneous membrane (Fig. 3) that is subject to thermally excited undulations.

Based on the (linearized) Helfrich energy (1), a Fourier analysis of height fluctuations $h(x,y)$ predicts the widely used relation between the Fourier spectrum $\hat{h}_{\mathbf{q}}$ of the membrane height in wave modes q, the bilayer's macroscopic bending rigidity κ and its lateral tension η (Seifert, 1997)

$$\langle|\hat{h}_{\mathbf{q}}^2|\rangle=\frac{k_BT}{A(\kappa q^4+\eta q^2)},\tag{12}$$

with A being the projected membrane area and k_BT denoting Boltzmann's constant and temperature, respectively. Due to the action of the barostat, the DPD membrane is tensionless and hence $\eta=0$. Fitting Eq. (12) to the temporally averaged Fourier spectrum of our simulated bilayers (see Fig. 4) yields the bending rigidity for a single simulation run. Varying the concentration ratio of the lipid species in 10% steps (lipids having a stiffness $\kappa_B^{\text{DPD}}=3\kappa_A^{\text{DPD}}=30k_BT$), yields the desired relation $\kappa(\phi)$.

To reduce uncertainties, we averaged κ for each ϕ over 10 independent simulations and further determined the standard deviation of the mean (Fig. 5). As a result, we observe that the

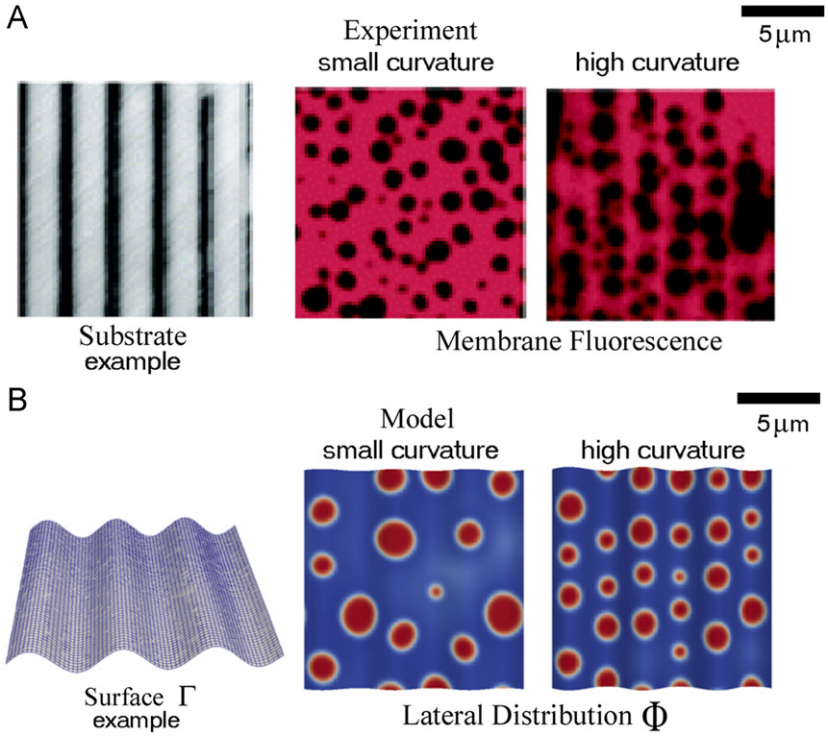

Fig. 2. Experiment and mathematical model. A: experimental curvature dependent phase separation in corrugated membranes (reprinted with permission from Parthasarathy et al. (2006), © 2006 American Chemical Society). B: simulations of the mathematical model coupling curvature with lateral phase separation. High curvatures induce an ordering, whereas phase separation on small curvatures appears randomly.

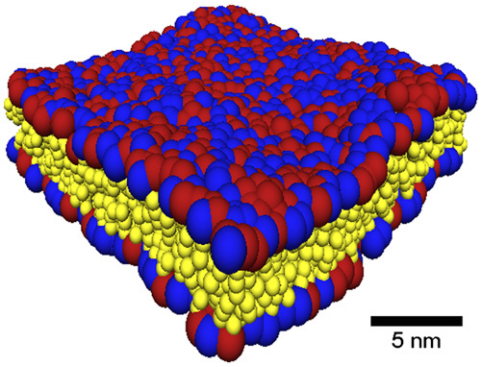

Fig. 3. Typical DPD simulation snapshot with $\langle\phi\rangle = 0$, i.e. a 1:1 ratio of lipid species A and B. The size of the patch corresponds to ~ 25 nm $\times$ 25 nm (cf. main text for details on the conversion from DPD to SI units). The simulation setup produced stable membranes in a tensionless state with thermally excited undulations. Blue and red spheres indicate lipid headgroups corresponding of lipids A and B, respectively; hydrophobic lipid chains are depicted in yellow. (For interpretation of the references to color in this figure legend, the reader is referred to the web version of this article.)

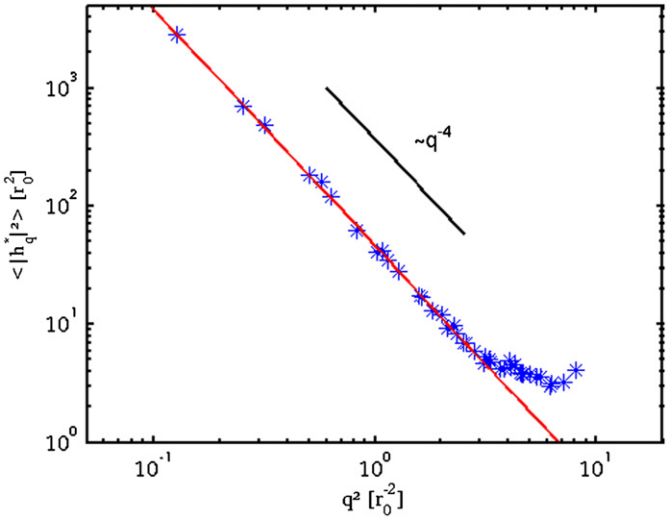

Fig. 4. The fluctuation spectrum of the DPD bilayers (symbols) is well fitted by Eq. (12) (full line). The anticipated scaling of a tensionless membrane is also indicated. For large wave vectors (given here as q^2), the spectrum is governed by protrusion modes that are not considered in the mean-field derivation of the fitting function.

bilayer's bending rigidity interpolates sigmoidal between the two limiting cases ($\phi = \pm 1$) in which only one lipid species is present. Starting from a pure bilayer composed of soft or stiff lipids only (i.e. $\phi = -1$ or $\phi = +1$) the addition of a small amount of the second lipid species leads only to minor changes in the bilayers bending rigidity. Only for comparable amounts of both lipid species a considerable deviation from the limiting cases is seen.

3.2. Macroscopic scale—finite element simulations

Using the calibrated functional relationship $\kappa(\phi)$ obtained by the DPD studies on a small scale level, we study numerically the lateral phase separation behavior in curved lipid bilayers on the large scale. Here, lateral phase separation is induced by gradients in the macroscopic elastic moduli κ,κ_G and H_0. The molecular pendant is differences in stiffness and shape of two kinds of membrane molecules.

In the first part, we compare the difference in dynamics and minimum patterns of our upscaled nonlinear function $\kappa(\phi)$ with common linear approximations. In the second part, we qualitatively and quantitatively compare and analyze the impact of gradients in each of the elastic moduli κ, κ_G and H_0 on lateral phase separation.

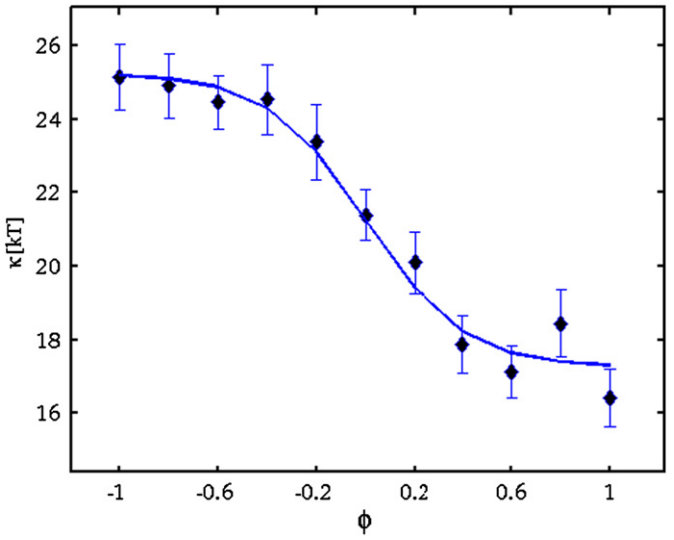

Fig. 5. The bending rigidity κ of the simulated bilayers varies sigmoidal with the concentration of lipid species, ϕ. Here, $\phi=\pm 1$ correspond to pure membranes consisting only of stiff or soft lipids (A,B), respectively. Lipid stiffness is here $\kappa_B^{DPD}=3\kappa_A^{DPD}=30k_bT$. Each data point reflects the mean of 10 simulations, error bars denote the standard deviation of the mean. While κ is barely affected by small changes in the lipid composition, similar concentrations of both lipids yield a massive change of the bilayer's bending properties. Full line is a heuristic fit $(a+b\tanh(-c\phi)$ with a=21.3, b=4.0 and c=2.5) that may serve as a guide to the eye.

Throughout this section we use the following setup: the space discretization Γ^q consists of J=4096 quadrangles with periodic boundary conditions for ϕ^m and Y^m. Since the Cahn–Hilliard functional has a small length scale, mesh sizes have been always chosen significantly smaller than the transition length. We numerically have proved an experimental order of convergence of 2 as the mesh sizes are reduced. To control if the used mesh size is sufficient to describe realistic dynamics and patterns, we have ensured that J=16 384 and J=65 536 quadrangles yield the same results. The time discretization is based on an adaptive time stepping scheme, starting with $\tau_0=0.3$ s. (Since available experimental data do not contain the full parameter set necessary to parameterize our model; some parameter values have to be estimated.) We have used a stochastically disturbed initial distribution $\phi^0=\phi(t=0)$ of total average $\langle\phi^0\rangle=\Phi^0$ over the domain. To assure the comparability of different simulations, always the same stochastically perturbed initial conditions have been used. Additionally, we have set: $\tilde{\sigma}=119.47k_BT\mu m^{-2}$, $\xi=0.133$ μm, $L_\phi=3.87\times10^{-4}$ μm^4 s$^{-1}(k_BT)^{-1}$ and for the double well potential we have chosen $f(\phi)=\frac{9}{32}(\phi^2-1)^2$. If not otherwise stated, we have considered $H_0^A=H_0^B=0$ μm^{-1}; $\kappa^A=\kappa^B=25.2k_BT$ and $\kappa_G^A=\kappa_G^B=-25.2k_BT$ ensuring the stability restriction $0\geq\kappa_G\geq-2\kappa$ (Schwarz and Gompper, 2002). This set of parameters implies the following molecular membrane diffusion coefficient $D=L_\phi\tilde{\sigma}=1.15\times10^{-10}$ cm^2 s^{-1} as well as the following 'sharp' line tension given by $\sigma=\tilde{\sigma}\xi=15.84k_BT\mu m^{-1}$ (Kwak, 2007). (Odd numbers result from the conversion of abstract nondimenzionalized model parameters into physical values.)

3.2.1. Parameterized model vs. linear approximations

Although the idea of coupling macroscopic elastic moduli with the lateral composition of lipid bilayers has been used in the past, the exact nature of these dependencies remains still unrevealed. Different approaches reaching from phenomenological coupling terms (Allain and Amar, 2006; Chen, 1999; Jiang et al., 2000; Taniguchi, 1996; Yin and Lv, 2008) to linear (Li et al., 2006) and nonlinear (Lowengrub et al., 2009; Wang and Du, 2008) functions $\kappa(\phi)$,$\kappa_G(\phi)$ and $H_0(\phi)$ have been used.

For the first time, a multiscale approach is proposed in this study. As an example the bending rigidity κ of the continuous model has been parametrized via DPD experiments. We find that $\kappa(\phi)$ has the form of a tanh-function (see Fig. 5) rather than a simple linear relationship. In order to get an impression of the importance using more realistic upscaled data, we have performed comparative studies: considering on the one hand the nonlinear (upscaled) function

$$\kappa_{\tanh}(\phi)=a+b_1\tanh(-\phi), \tag{13}$$

and on the other hand the linear case commonly adopted

$$\kappa_{\text{lin}}(\phi)=a+b_2\phi. \tag{14}$$

In Fig. 6 the corresponding results are shown. The constants $a=(\kappa^A+\kappa^B)/2$, $b_1=(\kappa^A-\kappa^B)/2\tanh(1)$ and $b_2=(\kappa^A-\kappa^B)/2$ are chosen such that in both cases $\kappa(1)=\kappa^A=17.3k_BT$ and $\kappa(-1)=\kappa^B=25.2k_BT$ is ensured. Furthermore, in both simulations we use the fixed geometry $\Gamma=\vec{X}(u_1,u_2)=0.625\sin(6\pi u_1)\mu$m (cf. Fig. 2B) and the initial conditions $\langle\phi^0\rangle=0$, i.e. a 1:1 mixture of both components. The prescribed geometry ensures $K\equiv0$ such that κ_G does not play any role for this specific geometry.

We observe in early states of phase separation in the nonlinear case of κ a stronger dependence on the curvature (Fig. 6C) than in the linear case (Fig. 6A). This is likely to be a consequence of the steeper gradient of κ_{tanh} compared to κ_{lin} close to the initial value $\langle\phi^0\rangle=0$. Since the breakage of already formed cross-connections between the phases is energetically costly (it would elongate the overall size of the boundaries) early sorting effects can trap the system into different minimum patterns, corresponding to local minima of the free energy (2). This becomes obvious in comparing the minimum configurations Fig. 6B with Fig. 6D.

Choosing initial conditions $\langle\phi^0\rangle$ away from zero, e.g. having much of one component and less of the other, does not result in different local minimum configurations (results not shown). Since in that case circular phases of the component with the smaller amount are quickly arising and stable cross-connecting phases (cf. green circular marks in Fig. 6A) are missing.

3.2.2. Gradients in elastic moduli and lateral sorting

So far we have only studied the influence of lipids with differences in the bending rigidity $\kappa(\phi)$, which has previously shown to induce lateral sorting. In the following, we also investigate the impact of spatial gradients in the spontaneous curvature H_0 and the Gaussian rigidity κ_G. Especially the latter has not been studied so far in the literature. To do so, the moduli are again assumed to be functions of the order parameter ϕ. Due to our results from the DPD studies we assume that the rigidity functions $\kappa(\phi)$ as well as $\kappa_G(\phi)$ have the form $a+b_1\tanh(-\phi)$. For the spontaneous curvature, we use the linear function $H_0(\phi)=a+b_2\phi$. In further studies one should of course try to identify κ_G as well as H_0 from DPD studies or other molecular approaches. Furthermore, for the following simulations we have chosen $\Gamma=\vec{X}(u_1,u_2)=0.75\sin(4\pi u_1)\sin(4\pi u_2)$ μm (cf. Fig. 7L) and $\langle\phi^0\rangle=-0.6$.

In the following, the notation Δh depicts the difference $|h^A-h^B|$ in an elastic modulus $h\in\{\kappa,\kappa_G,H_0\}$ between the two species A and B. Interestingly, varying independently all three elastic moduli in our simulations we observe in principle the same effects: the stronger Δh the faster phase separation occurs. This can be observed by an early and faster decay of the Cahn–Hilliard part F_2 of the free energy from the instable initial conditions (cf. Fig. 7A–C). Plotting the time T_{min} required to achieve the minimum against Δh yields in all cases an exponential decay of $T_{min}(\Delta h)$ (cf. Fig. 7D–F). The exponential fit leads to

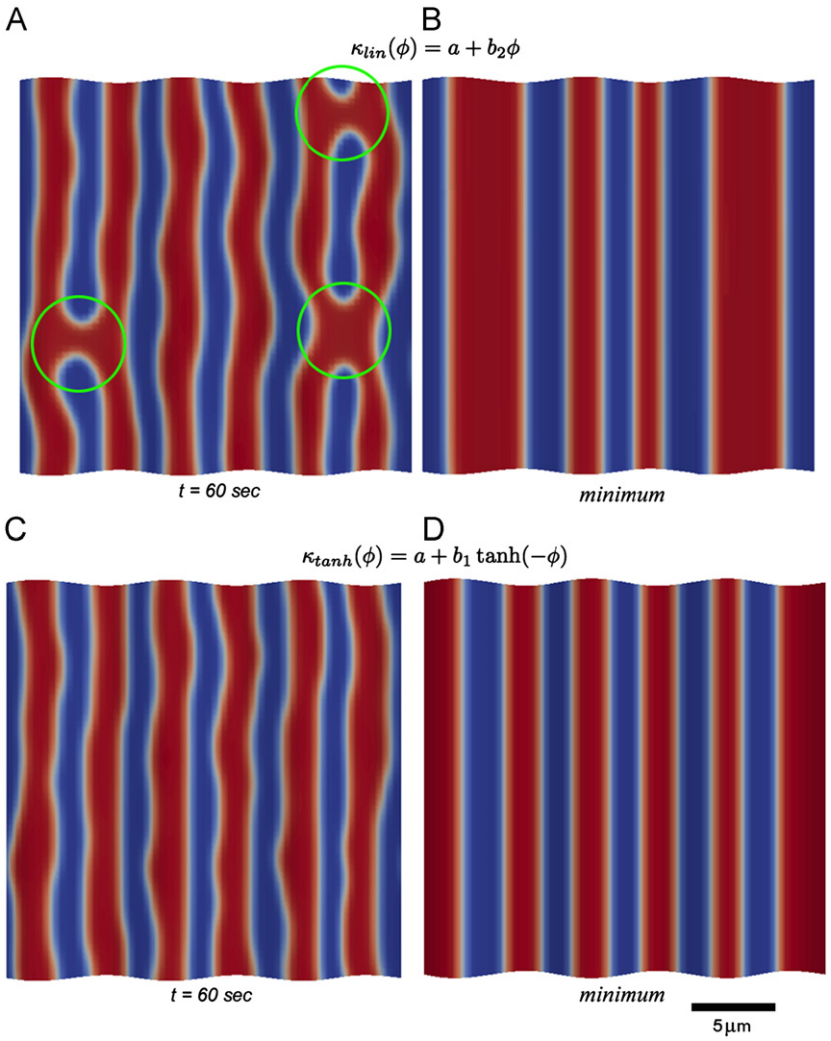

Fig. 6. Different minimum patterns depending on the form of the function $\kappa(\phi)$. A–B: κ is linear; C–D: κ is a form of $a+b\tanh(-\phi)$. Note that early sorting in (A) is less curvature dependent than in (C), showing cross-connections between the red domains (green circular marks). (For interpretation of the references to color in this figure legend, the reader is referred to the web version of this article.)

a good approximation for physically reasonable values, but for significantly larger values we observe that T_{min} decays even stronger, approaching the axis without any offset (as used in the exponential fit).

In the case $\Delta\kappa = \Delta\kappa_G = \Delta H_0 = 0$, phase separation occurs randomly (results not shown). Considering gradients in each of the moduli distinct curvature dependent phase separation patterns can be observed: choosing nonzero $\Delta\kappa_G$ induces phase separation of the component with the lower absolute value of κ_G in areas with high negative Gaussian curvature (Fig. 7H). Doing the same with $\Delta\kappa$ we observe phase separation of the component with the lower bending rigidity in regions with high mean curvature (Fig. 7G). Choosing $H_A < 0$ while $H_B = 0$ (causing $\Delta H_0 \neq 0$) drives ϕ_A to regions allocating this curvature (Fig. 7I). Interestingly in most of the cases these minimum patterns are only metastable, showing only slight changes in the size of the domains for a long time after T_{min}, but resulting very late ($t > 300$ min) in different minimum patterns with less and larger domains (cf. Section 3.2.4).

The observed minimum patterns (cf. Fig. 7G–I) differ significantly—each minimum pattern is the optimal pattern for the considered corresponding elastic modulus. Therefore, it is absolutely necessary to consider all three effects if one is interested in biological applications, since neglecting one part could lead to completely different minimum patterns and thus different biological interpretations.

3.2.3. Curvature gradients and lateral sorting

Curvature depending sorting in membranes appears to be the result of the interplay between spatial gradients in the elastic moduli and in membrane curvature (Parthasarathy et al., 2006). In the previous section we have varied the strength of spatial moduli gradients, keeping the membrane geometry constant. In this section we vary the membrane geometry (i.e. the strength of curvature gradients) keeping differences in the elastic moduli constant. Corresponding results are shown in Fig. 8. In order to quantify curvature gradients in mean curvature H and Gaussian curvature K, we define $H'_{max} := \max\{|\nabla^{\Gamma}[H(\vec{X})]| : \vec{X} \in \Gamma\}$ as well as $K'_{max} := \max\{|\nabla^{\Gamma}[K(\vec{X})]| : \vec{X} \in \Gamma\}$. Since these are global quantities, all following relationships in this regard are inherently global.

First, we fix for each elastic modulus $h \in \{\kappa, \kappa_G, H_0\}$ a certain difference $\Delta h \neq 0$ (while choosing vanishing differences in the other two moduli) but varying the corresponding curvature gradient $G'_{max} \in \{H'_{max}, K'_{max}\}$. We observe in all three cases, the stronger G'_{max} is the earlier and faster phase separation occurs (cf. Fig. 8A–C). Plotting the time to the achievement of the

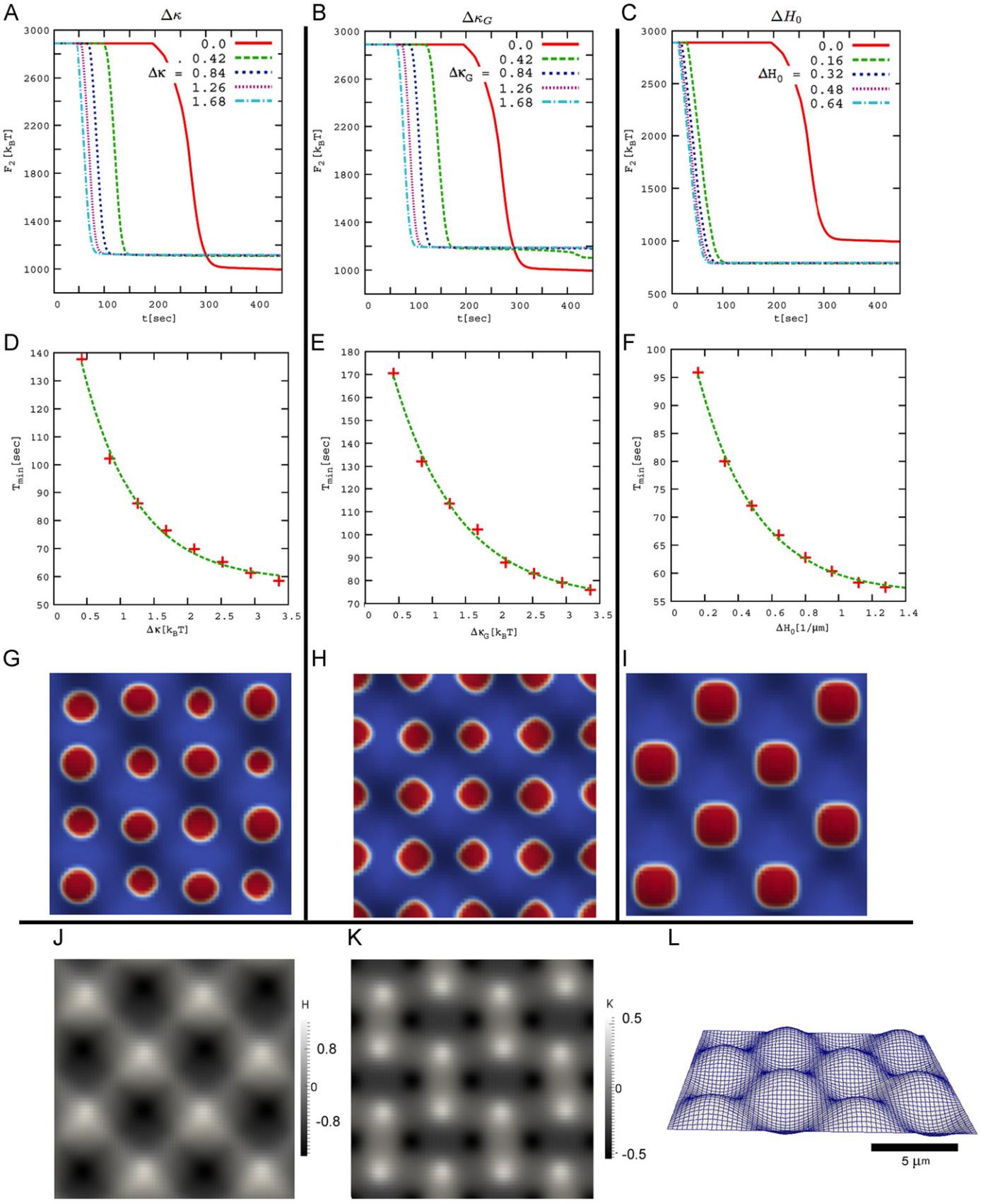

Fig. 7. Investigating lateral sorting using different strengths of gradients in the elastic moduli $\Delta\kappa$ (A,D,G), $\Delta\kappa_G$ (B,E,H) and ΔH_0 (C,F,I) on a fixed nonplanar surface. A–C: the decay of the Cahn–Hilliard energy F_2 in time. The stronger Δh ($h \in \{\kappa, \kappa_G, H_0\}$), is the earlier is the observed decay of F : 2. D–F: the time up to the metastable pattern T_{min} decays exponentially with Δh (red dots: values from simulations; green spotted line: exponential fit of the kind $a+b\exp(-c\Delta h)$. For significantly larger Δh-values we observe that T_{min} decays even stronger, approaching the axis without any offset). G–I: representative minimum patterns. J: mean curvature of Γ. K: Gaussian curvature of Γ. L: discretized surface Γ, side view. (For interpretation of the references to color in this figure legend, the reader is referred to the web version of this article.)

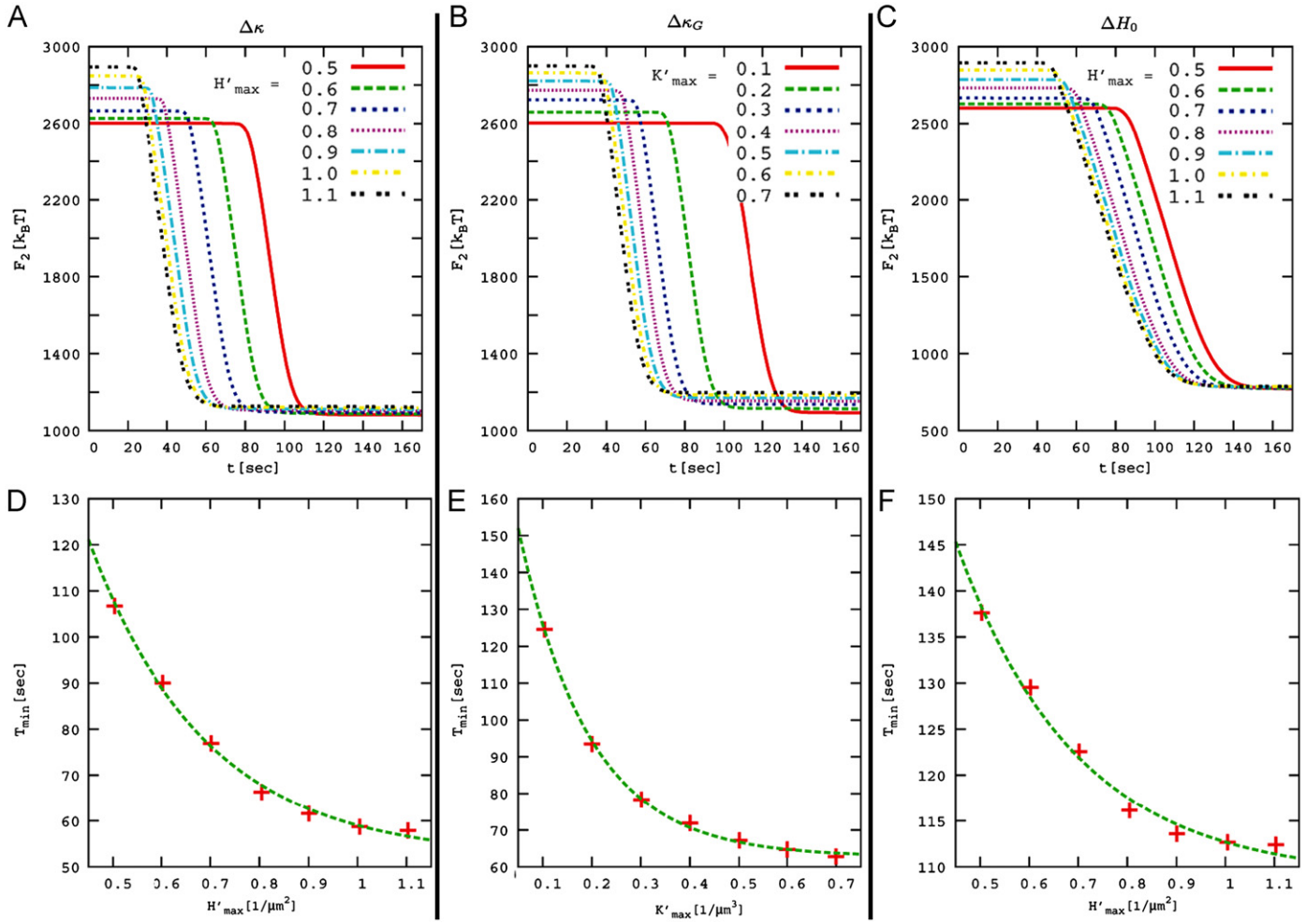

Fig. 8. Investigating lateral sorting using different strengths of curvature gradients $G'_{max} \in \{H'_{max}, K'_{max}\}$ but fixed differences in the elastic moduli $\Delta\kappa \neq 0$ (A,D), $\Delta\kappa_G \neq 0$ (B,E) and $\Delta H_0 \neq 0$ (C,F). A–C: the decay of the Cahn–Hilliard energy F_2 in time. The stronger G'_{max} is, the earlier is the observed decay of F_2. D–F: the time up to the metastable pattern T_{min} decays exponentially with G'_{max} (red dots: values from simulations; green spotted line: exponential fit of the kind $a+b\exp(-c\Delta h)$. (For interpretation of the references to color in this figure legend, the reader is referred to the web version of this article.)

minimum T_{min} against the strength of G'_{max} yields in all cases an exponential decay of $T_{min}(G'_{max})$ (cf. Fig. 8D–F). In detail we have set $\Delta\kappa = 0.02 k_B T$ and $\Delta\kappa_G = \Delta H_0 = 0$ in Fig. 8A and D; $\Delta\kappa_G = 0.02 k_B T$ and $\Delta\kappa = \Delta H_0 = 0$ in Fig. 8B and E as well as $\Delta H_0 = 0.08\ \mu m^{-1}$ and $\Delta\kappa = \Delta\kappa_G = 0$ in Fig. 8C and E.

Hence, increasing differences in elastic moduli as well as increasing gradients in membrane curvature accelerate the lateral sorting process exponentially.

3.2.4. *Parameter interplay and its influence on the stability of sorting patterns*

As mentioned above, most of the observed curvature depending patterns appear to be metastable: if differences in elastic moduli and curvature gradients are strong enough, a periodic symmetric pattern appears at $t = T_{min}$, which loses at $t = T_{max}$ its symmetry by fusing to less and bigger domains. The latter can be observed by a jump in the free energy F_2 (cf. Fig. 9A). This process continues stepwise; the assumed stable minimum pattern is built up of one big domain. To quantify the stability of a curvature modulated pattern, we define $T_{stab} := T_{max} - T_{min}$ which equals to zero if no curvature depending sorting takes place. In order to quantify the chemo-mechanical disposition for curvature modulated sorting subject to line tension and modulus contrast, for each $h \in \{\kappa, \kappa_G, H_0\}$ we introduce the elastic parameter $\chi^h_{el} = \Delta h/\sigma$ (Rózycki et al., 2008). We systematically investigate the influence of gradients in elastic moduli, line tension and curvature gradients on the stability T_{stab}. To do so, for each modulus h and the corresponding curvature gradient $G'_{max} \in \{H'_{max}, K'_{max}\}$ we have performed ≥ 25 simulations with different parameter sets (G'_{max}, χ^h_{el}). Our results clearly show, that increased values for G'_{max} as well as for χ^h_{el} result in an increased stability T_{stab} (cf. Fig. 9B–D).

For each $h \in \{\kappa, \kappa_G, H_0\}$ we present phase diagrams, showing regions with at least metastable curvature modulated pattern formation (CP) and curvature independent sorting regions (CIP) relying on χ^h_{el} and the corresponding $G'_{max} \in \{H'_{max}, K'_{max}\}$ (cf. Fig. 9E–G). To do so, we assume that the relation $\chi^h_{el} = \tilde{f}^h_{tr}(G'_{max})$ describing the transition between CP and CIP regions can be approximated by $f^h_{tr}(G'_{max}) = a/G'_{max} + b/(G'_{max})^2$ for $a,b \in \mathbb{R}_{\geq 0}$. This is physically motivated by the assumption that the *graph*$(\tilde{f}^h_{tr})$ asymptotically approaches the axes. Based on our numerical simulations, heuristic fits yield rough approximations of $\tilde{f}^h_{tr}$ (blue spotted lines in Fig. 9E–G). (Fits are based on the least square method, using simulations within the $G'_{max} - \chi^h_{el}$-space, showing small values $T_{stab} > 0$.) Especially it holds $f^{\kappa}_{tr}(H'_{max}) = 0.0043/H'_{max} + 0.0052/(H'_{max})^2$, $f^{\kappa_G}_{tr}(K'_{max}) = 0.0048/K'_{max}$ as well as $f^{H_0}_{tr}(H'_{max}) = 0.00023/H'_{max}$. In future experiments these functions can be used

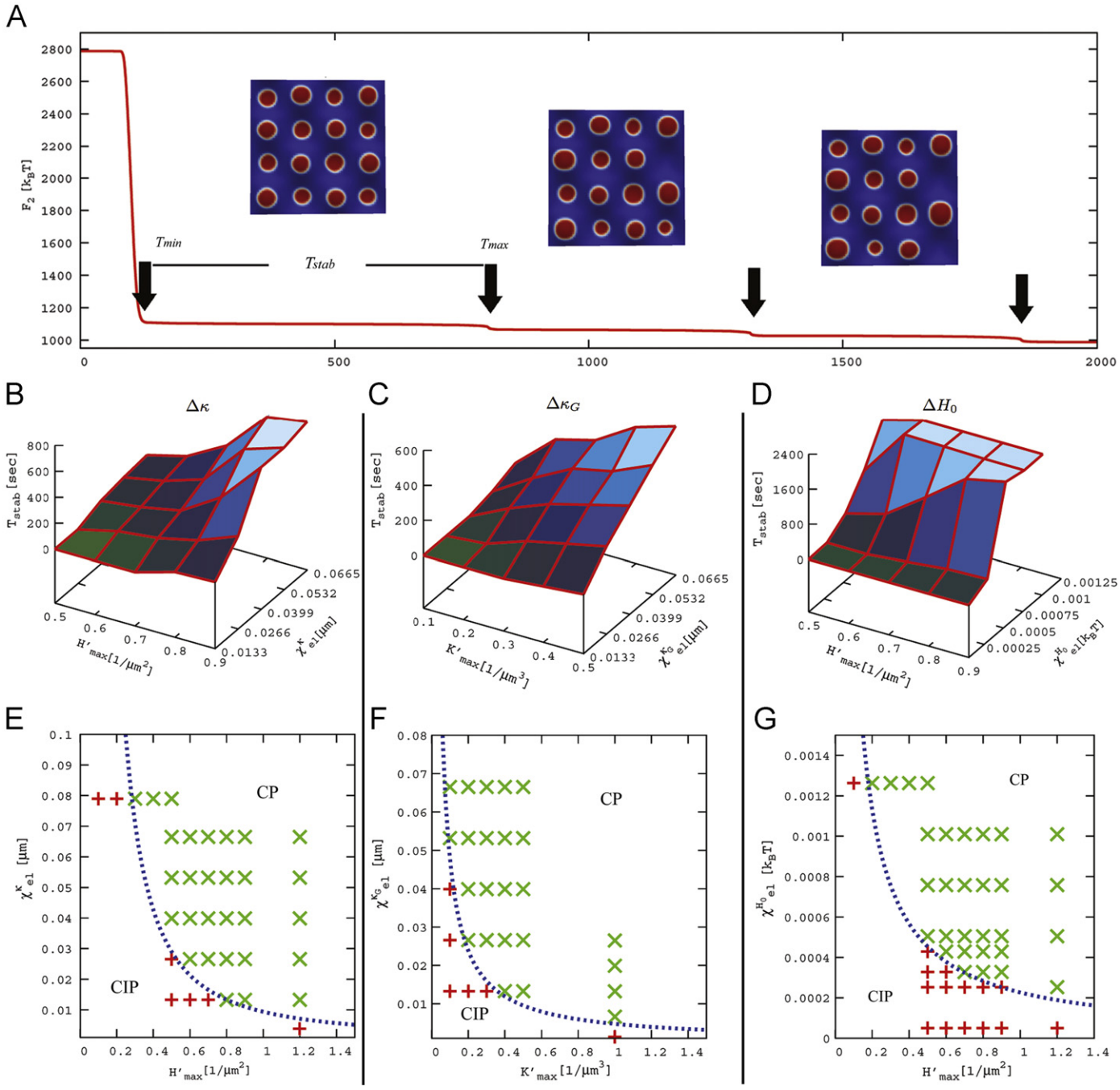

Fig. 9. Stability of patterns depending on the interplay of elastic moduli gradients, curvature gradients and the line tension. A: simulation example, $T_{stab} \coloneqq T_{max} - T_{min}$ measures the stability of a curvature modulated pattern, where T_{max} defines the time where the symmetry of the pattern gets lost by fusing domains. Each fusion can be recognized by a jump in the free energy F_2 (black arrows). B–D: for each $h \in \{\kappa, \kappa_G, H_0\}$, T_{stab} increases with growing curvature gradient H'_{max} and K'_{max}, respectively, as well as with growing corresponding elastic parameter $\chi^h_{el} = \Delta h/\sigma$ (in (D) the value T_{stab} has been catted at $T_{stab} = 2400\ s$ due to limited simulation time). E–G: phase diagrams as a function of the elastic parameter χ_{el} for each elastic modulus and the corresponding curvature gradient. CP: region with (metastable) curvature modulated sorting, CIP: region with curvature independent sorting. Green x-marks: simulations with $T_{stab} > 0$, red +-marks: simulations with $T_{stab} = 0$. Blue dotted line: heuristically fitted transition line of the kind $a/x + b/x^2$. (For interpretation of the references to color in this figure legend, the reader is referred to the web version of this article.)

to estimate if curvature modulated sorting will occur. This is the case namely if for at least one elastic modulus h the relationship $\chi^h_{el} \gg f^h_{tr}(G'_{max})$ holds for the corresponding value $G'_{max} \in \{H'_{max}, K'_{max}\}$.

4. Discussion

In the present paper, we have outlined a continuous multiscale model for curvature induced lateral sorting in biological membranes. Passive lateral organization in membranes is involved and actually is a premiss for various cellular processes, such as budding (Baumgart et al., 2003), signaling (Sugar et al., 2001) and sorting (Lee, 2005). Furthermore, it is assumed to be a condition precedent for the biogenesis and maintenance of cellular organelles itself (Mullins, 2005). Thus it is critical for the function of each biological cell. The presented model enables to study the impact on dynamics and minimum patterns if two membrane components differ in at least one of the macroscopic elastic moduli. Here, we have studied the influence of curvature gradients in interplay with the bending rigidity κ, the

spontaneous curvature H_0 and the Gaussian rigidity κ_G. The latter has not been studied in the literature so far. In terms of molecular parameters the different elastic moduli reflect differences in stiffness and shape of the corresponding molecules.

Differences in the elastic moduli have been experimentally used to study the interplay between molecular properties and curvature (Baumgart et al., 2003; Heinrich et al., 2010; Kamal et al., 2009; Parthasarathy et al., 2006; Pencer et al., 2008; Roux et al., 2005; Tian and Baumgart, 2009; Yoon et al., 2006). Furthermore, various theoretical continuous approaches have already been used to study the coupling of different moduli with curvature (Allain and Amar, 2006; Chen, 1999; Jiang et al., 2000; Li et al., 2005; Lowengrub et al., 2009; Taniguchi, 1996; Wang and Du, 2008; Yin and Lv, 2008; Elliott and Stinner, 2010). Despite of this effort, four points have not been studied so far (at least up to our knowledge):

(1) Parameterization of the presented continuous model directly from the molecular scale.
(2) Studies of the influence of differences in the Gaussian rigidities on lateral sorting.
(3) Phase diagrams estimating if and how stable curvature depending sorting will occur.
(4) Proofs concerning the existence and uniqueness of a solution for presented models.

In this study we have addressed these four gaps.

First of all, we have studied the influence of the detailed parametrization, i.e. the functional dependencies used in the model. To do so, we have used DPD to determine the dependence of the bending rigidity $\kappa(\phi)$ on the composition of a binary lipid bilayer. We have restricted ourselves to lipids of the same length and type yet varied the lipids chain stiffness. This approach e.g. reflects a flexible poly-*cis* unsaturated membranes and stiffer saturated/monounsaturated phosphatidylcholine (PC) lipids (Rawicz et al., 2000). Furthermore, this case is of special interest for the finite element simulations, because the calculation of the free energy requires microscopically well-mixed system. As a result, we have found that the bending rigidity is only weakly affected when minor amounts of a different lipid type are introduced. For intermediate lipid concentrations, i.e. roughly a 1:1 ratio of lipids, however a strong deviation from the limiting case of pure membranes has been observed. Indeed, $\kappa(\phi)$ is best described by a sigmoid curve, e.g. having a tanh-form.

It has been previously shown that the functional relationship $\kappa(\phi)$ can be nonlinear, depending on different molecular properties of membrane molecules (Brannigan and Brown, 2005; Illya et al., 2006; Szleifer et al., 1988). In the macroscopic finite element simulations, we have found that the steady state depends strongly on the exact choice of $\kappa(\phi)$. In Fig. 6 the dynamics and minimum configurations of two simulations are shown comparing the use of a linear bending rigidity $\kappa_{lin}(\phi)$ with the nonlinear case $\kappa_{tanh}(\phi)$. The latter has been determined directly from DPD studies. Although the global energy F of a given lateral distribution ϕ on Γ is the same for the two cases κ_{lin},κ_{tanh}, we observe strong differences in dynamics and minimum patterns. We postulate that this effect is due to differences in $(d/d\phi)\kappa_{lin}$ and $(d/d\phi)\kappa_{tanh}$, leading locally (and very early in time) to differences in the strength of curvature dependent sorting. This again traps the whole system in completely different minimum patterns. These results emphasize the importance of dynamics and parameters in mathematical modeling. That is, even if only minimum patterns (with a certain set of parameters) are studied, one should carefully check, the dependence of the minimum configuration on initial conditions as well as the robustness with respect to parameter variation.

Furthermore, the impact of differences in each of the macroscopic elastic moduli on lateral sorting has been investigated using macroscopic finite element simulations (cf. Fig. 7). Our results suggest that each of the moduli κ, H_0 and κ_G has a comparable impact on dynamics and curvature dependent patterns: in the parameter regime studied the decomposition time decreases roughly exponentially with the gradient of each elastic modulus. The same effect can be observed by fixing the difference in each elastic modulus and increasing corresponding curvature gradients (cf. Fig. 8). Additionally, each gradient can lead to a distinct minimum pattern, influenced by the mean curvature or the Gaussian curvature of the given geometry, respectively. These findings suggest that the Gaussian rigidity plays an equivalent role in lateral sorting, as the other two moduli, which are well known to influence lateral sorting (Allain and Amar, 2006; Baumgart et al., 2003; Chen, 1999; Heinrich et al., 2010; Jiang et al., 2000; Kamal et al., 2009; Li et al., 2005; Lowengrub et al., 2009; Parthasarathy et al., 2006; Pencer et al., 2008; Roux et al., 2005; Taniguchi, 1996; Tian and Baumgart, 2009; Wang and Du, 2008; Yoon et al., 2006; Yin and Lv, 2008).

The presented results agree with the following molecular intuition: given an arbitrary curved membrane containing a stiff and a flexible component, it is energetically favorable for the more flexible component to stay in curved regions, independent of the sign of the principle curvatures. To account for each kind of curvature, we have to consider both, gradients in the bending rigidity and in the Gaussian rigidity (cf. Fig. 1).

These findings are supported by the experimental observation that differences in bending rigidities usually coincide with differences in Gaussian rigidities (Semrau et al., 2008). The importance of the elusive Gaussian rigidity in biological processes has been neglected for a long time. Only very recently theoretical studies investigate its influence on membrane shapes (Baumgart et al., 2005; Brannigan and Brown, 2007; Das et al., 2009), fusion (Siegel, 2008) and lateral diffusion (Yoshigaki, 2007) considering either a homogeneous membrane composed of only one component or – in the case of two component membranes – domains composed of different molecular species have been assumed to be lateral immobile. In experiments investigating lateral sorting, effects due to Gaussian rigidities are also generally assumed to be negligible (Yoon et al., 2006). This may be caused by the fact that on the one hand κ_G cannot be measured directly in experiments (Siegel and Kozlov, 2004) and on the other hand the Gauss–Bonnet Theorem (stating $\int_S K\, d\omega = const$ in homogeneous materials considering closed membranes) may have led to a misunderstanding, that the effect of K is negligible in heterogeneous membranes as well. However, the results presented in this study show that the impact of inhomogeneities in Gaussian rigidities have a comparable strong effect on lateral sorting compared with the other two moduli, the bending rigidity and the spontaneous curvature.

The results presented in Fig. 9 show that the appearance and stability of curvature modulated patterns strongly depends on the exact choice of line tension, curvature gradients and moduli gradients. The question if beside metastable patterns also stable curvature modulated patterns exist, has to be traced by methods of rigorous stability analysis and is far beyond the scope of this paper. But the presented phase diagrams and corresponding approximations of transition boundaries in this study allow to estimate at least, under which conditions curvature modulated sorting takes place.

In addition to the computational studies, we have outlined the proof of existence and uniqueness for the macroscopic model yielding the well-posedness and the boundedness of a

solution. Thus we have ensured that the numerical simulations indeed provide the approximation of the unique solution of the considered problem. The structure of the nonlinear function f and the assumptions on κ, H_0, κ_G guarantee the global existence of a solution in contrast to the existence of a blow up in finite time for the Cahn–Hilliard equation choosing different functions f, see Elliott and Songmu (1986).

To sum up, an extended continuous multiscale model for curvature modulated sorting in biological membranes has been proposed. Particularly the model enables to study curvature depending lateral sorting of different components as a result of differences in their mechanical properties (such as the shape and the stiffness). The model is given in terms of a nonlinear PDE of fourth order, the existence of a unique solution has been shown analytically. Furthermore, we have presented simulations using a finite element approach and have derived detailed functional relationships from the molecular level using DPD studies. Our simulations show that gradients in the three elastic moduli result in distinct metastable minimum patterns significantly different for each modulus, and that the decomposition time decreases exponentially with increasing difference in the modulus or corresponding curvature gradient. Additionally we have shown that the stability of curvature modulated patterns increases with increasing moduli- or curvature gradients. Presented phase diagrams allow to estimate if curvature modulated sorting will occur for set of geometry and elastic parameters.

In the future, all these findings can help to understand, predict and interpret more precisely experimental observations concerning curvature dependent lateral organization and its stability in biological membranes.

Acknowledgments

The authors would like to thank the anonymous reviewers for their suggestions and comments which have significantly improved the presentation of this paper. The authors greatly thank Anna Marciniak-Czochra and Ansgar Bohmann for scientific support. We acknowledge financial support of the ViroQuant Project (German FORSYS initiative) and the Akademie der Wissenschaften, Heidelberg.

Appendix A

In this section we present the details on the proof of existence and uniqueness of a solution of the problem (4)–(6), stated in Theorem 3.

Proof of Theorem 3 Existence. To show the existence of a weak solution of (4)–(6) we use the Galerkin method and look for a function $\phi^k(t,x)=\sum_{i=1}^k \alpha_i^k(t)w_i(x)$ satisfying Eq. (8) and initial condition $\phi^k(0)=\phi_0^k$. Using the properties of the basis $\{w_i\}_{i\in\mathbb{N}}$ we obtain that for each $k\in\mathbb{N}$ the function ϕ^k is determined by the solution $(\alpha_1^k(t),\dots\alpha_k^k(t))$ of an initial value problem for a system of ordinary differential equations

$$\frac{d}{dt}\alpha_j^k = -\alpha_j^k L_\phi \tilde{\sigma}\xi^2\int_\Gamma |\Delta^\Gamma w_j|^2\,d\omega - L_\phi\int_\Gamma \nabla^\Gamma R\left(\sum_{i=1}^k \alpha_i^k(t)w_i(x),H,K\right)\times\nabla^\Gamma w_j\,d\omega,$$

$$\alpha_j^k(0)=(\phi_0,w_j)_{L^2(\Gamma)},\quad j=1,\dots,k. \tag{15}$$

The right hand side in (15) is locally Lipschitz-continuous in α_j^k and a unique local solution exists. The estimate $\operatorname{esssup}_{(0,T)}\|\phi^k\|_{L^2(\Gamma)}\le C$, proved in Lemma 4, implies the boundedness of $(\alpha_1^k,\dots,\alpha_k^k)$ and the existence of a global solution of (15).

From a priori estimates, shown in Lemma 4, follows the existence of a function $\phi\in L^2(0,T;H^2(\Gamma))\cap H^1(0,T;L^2(\Gamma))$, $\phi\in L^\infty((0,T)\times\Gamma)$, and a subsequence (denoted again by $\{\phi^k\}$) such that $\phi^k\rightharpoonup\phi$ in $L^2(0,T;H^2(\Gamma))$, $\partial_t\phi^k\rightharpoonup\partial_t\phi$ in $L^2((0,T)\times\Gamma)$, $\phi^k\overset{*}{\rightharpoonup}\phi$ in $L^\infty((0,T)\times\Gamma)$ as $k\to\infty$.

Using Lions–Aubin Lemma, Lions (1969), and compact embedding of $H^2(\Gamma)$ in $H^1(\Gamma)$ (Hebey, 1996, p. 24), we obtain the strong convergence $\phi^k\to\phi$ in $L^2(0,T;H^1(\Gamma))$ and $\phi^k\to\phi$ a.e. in $(0,T)\times\Gamma$ as $k\to\infty$. Due to $\phi\in H^1(0,T;L^2(\Gamma))$ we have $\phi\in C([0,T];L^2(\Gamma))$ and $\phi^k(0)\to\phi(0)$ in $L^2(\Gamma)$ implies $\phi(0)=\phi_0$ in $L^2(\Gamma)$.

Due to assumptions on κ, H_0, κ_G and boundedness of ϕ^k we obtain that R, $\partial_H R$, $\partial_\phi R$ and $\partial_K R$ are continuous and bounded. The convergence of ϕ^k implies $R(\phi^k,H,K)\to R(\phi,H,K)$, $\partial_\phi R(\phi^k,H,K)\to\partial_\phi R(\phi,H,K)$, $\partial_H R(\phi^k,H,K)\to\partial_H R(\phi,H,K)$, $\partial_K R(\phi^k,H,K)\to\partial_K R(\phi,H,K)$ a.e. in $(0,T)\times\Gamma$ and the weak convergences $R(\phi^k,H,K)\rightharpoonup R(\phi,H,K)$, $\partial_\phi R(\phi^k,H,K)\rightharpoonup\partial_\phi R(\phi,H,K)$, $\partial_H R(\phi^k,H,K)\rightharpoonup\partial_H R(\phi,H,K)$, $\partial_K R(\phi^k,H,K)\rightharpoonup\partial_K R(\phi,H,K)$ in $L^4((0,T)\times\Gamma)$ as $k\to\infty$.

Now for fix $m\in\mathbb{N}$, $m<k$, we take $v\in C^1([0,T];H^2(\Gamma))$ of the form $v=\sum_{i=1}^m d_i(t)w_i$ as a test function in (8), where d_i are given smooth functions. Then we integrate Eq. (8) with respect to t and pass to the limit as $k\to\infty$. For the linear terms we can use the weak convergence of ϕ^k directly. The nonlinear term we rewrite as

$$\begin{aligned}&\int_0^T\int_\Gamma(\partial_\phi R(\phi^k,H,K)\nabla^\Gamma\phi^k+\partial_H R(\phi^k,H,K)\nabla^\Gamma H\\&\quad+\partial_K R(\phi^k,H,K)\nabla^\Gamma K)\nabla^\Gamma v\,d\omega\,dt\\&=\int_0^T\int_\Gamma(\partial_\phi R(\phi^k,H,K)(\nabla^\Gamma\phi^k-\nabla^\Gamma\phi)\nabla^\Gamma v\\&\quad+\partial_\phi R(\phi^k,H,K)\nabla^\Gamma\phi\nabla^\Gamma v)\,d\omega\,dt\\&\quad+\int_0^T\int_\Gamma(\partial_H R(\phi^k,H,K)\nabla^\Gamma H+\partial_K R(\phi^k,H,K)\nabla^\Gamma K)\nabla^\Gamma v\,d\omega\,dt.\end{aligned}$$

In the first integral we use the strong convergence of ϕ^k in $L^2(0,T;H^1(\Gamma))$ and boundedness of $\partial_\phi R(\phi^k,H,K)$, in all other terms the weak convergence in $L^4((0,T)\times\Gamma)$ and the embedding of $L^\infty(0,T;H^2(\Gamma))$ in $L^4(0,T;W^{1,4}(\Gamma))$ for $\dim(\Gamma)\le 3$ are applied. Using now the fact that all functions v of the considered form are dense in $L^2(0,T;H^2(\Gamma))$ we obtain that ϕ is a weak solution of the problem (4)–(6). □

In the next Lemma, we show the a priori estimates which are essential for the proof of existence and uniqueness. Additionally, these estimates imply the boundedness of a solution of (4)–(6).

Lemma 4. *Any weak solution of* (4)–(6) *satisfies the following a priori estimates*:

$$\begin{aligned}&\|\phi\|_{L^\infty(0,T;H^1(\Gamma))}+\|\Delta^\Gamma\phi\|_{L^\infty(0,T;L^2(\Gamma))}+\|(\Delta^\Gamma)^2\phi\|_{L^2((0,T)\times\Gamma)}\le C,\\&\|\partial_t\phi\|_{L^2((0,T)\times\Gamma)}\le C,\\&\|\phi\|_{L^\infty((0,T)\times\Gamma)}\le C,\quad \|\nabla^\Gamma\phi\|_{L^2(0,T;L^\infty(\Gamma))}\le C,\end{aligned} \tag{16}$$

where C is a universal constant independent of ϕ.

Proof of Lemma 4. Similar ideas for the proof of a priori estimates for the Cahn–Hilliard equation, defined in a bounded domain of dimension less or equal three, have been considered in Elliott and Songmu (1986). However, a generalization of this proof is necessary due to the nonlinear curvature-dependent terms in Eq. (4), defined on a smooth Riemannian manifold Γ. First, we show the estimates for the approximation sequence $\{\phi^k\}$. Then, the convergence of a subsequence of $\{\phi^k\}$ and the lower semi-continuity of norms will imply the corresponding estimates for ϕ. In order to obtain the estimate for $\nabla^\Gamma\phi^k$ in $L^\infty(0,T;L^2(\Gamma))$,

we consider

$$P(\phi^k)=\frac{1}{2}\kappa(\phi^k)(H-H_0(\phi^k))^2+\kappa_G(\phi^k)K+\tilde{\sigma}f(\phi^k),\quad P'(\phi^k)=R(\phi^k,H,K),$$

and the free energy

$$E(\phi^k)=\frac{1}{L_\phi}\int_\Gamma\left(P(\phi^k)+\frac{1}{2}\tilde{\sigma}\xi^2|\nabla^\Gamma\phi^k|^2\right)d\omega,$$

with

$$\frac{d}{dt}E(\phi^k)=\frac{1}{L_\phi}\int_\Gamma(R(\phi^k,H,K)\partial_t\phi^k+\tilde{\sigma}\xi^2\nabla^\Gamma\phi^k\nabla^\Gamma\partial_t\phi^k)\,d\omega. \tag{17}$$

The assumptions on f, κ, H_0, κ_G, H and K imply

$$P(\xi)\geq C(|\xi|^4-2|\xi|^2-|\xi|^3-|\xi|-1).$$

Using Eq. (8) and zero-flux boundary conditions, we rewrite the integral in (17) by

$$\begin{aligned}
&\int_\Gamma(R(\phi^k)(-\tilde{\sigma}\xi^2(\Delta^\Gamma)^2\phi^k+\Delta^\Gamma R(\phi^k))-\tilde{\sigma}\xi^2\Delta^\Gamma\phi^k(-\tilde{\sigma}\xi^2(\Delta^\Gamma)^2\phi^k\\
&\quad+\Delta^\Gamma R(\phi^k)))\,d\omega\\
&=-\int_\Gamma(|\nabla^\Gamma R(\phi^k)|^2-\tilde{\sigma}\xi^2\nabla^\Gamma\Delta^\Gamma\phi^k\nabla^\Gamma R(\phi^k)+\tilde{\sigma}^2\xi^4|\nabla^\Gamma\Delta^\Gamma\phi^k|^2\\
&\quad-\tilde{\sigma}\xi^2\nabla^\Gamma\Delta^\Gamma\phi^k\nabla^\Gamma R(\phi^k))\,d\omega+\int_{\partial\Gamma}(R(\phi^k)(\nabla^\Gamma R(\phi^k)\\
&\quad-\tilde{\sigma}\xi^2\nabla^\Gamma\Delta^\Gamma\phi^k)\cdot\nu-\tilde{\sigma}\xi^2\Delta^\Gamma\phi^k(\nabla^\Gamma R(\phi^k)-\tilde{\sigma}\xi^2\nabla^\Gamma\Delta^\Gamma\phi^k)\cdot\nu)\,d\varsigma\\
&=-\int_\Gamma(\tilde{\sigma}\xi^2\nabla^\Gamma\Delta^\Gamma\phi^k-\nabla^\Gamma R(\phi^k))^2\,d\omega\leq 0.
\end{aligned}$$

Here, we have used the shorted notation $R(\phi^k)$ for $R(\phi^k,H,K)$. Thus, $(d/dt)E(\phi^k)\leq 0$ and

$$\int_\Gamma\left(\frac{1}{2}\tilde{\sigma}\xi^2|\nabla^\Gamma\phi^k|^2+P(\phi^k)\right)d\omega\leq\int_\Gamma\left(\frac{1}{2}\tilde{\sigma}\xi^2|\nabla^\Gamma\phi_0^k|^2+P(\phi_0^k)\right)d\omega.$$

Using the structure of f, the assumptions on κ, H_0, κ_G, the estimate $|u|+u^2+|u|^3\leq\delta u^4+C_\delta$, the regularity of initial conditions, and the embedding $H^2(\Gamma)\subset L^4(\Gamma)$ for compact $\overline{\Gamma}$ with $n=\dim(\Gamma)\leq 3$, see Aubin (1998) and Hebey (1996), we obtain that ϕ_0^k is uniformly bounded in $H^1(\Gamma)\cap L^4(\Gamma)$ and

$$\sup_{(0,T)}\int_\Gamma(|\nabla^\Gamma\phi^k|^2+|\phi^k|^4)\,d\omega\leq C.$$

Then, the Sobolev embedding theorem (Aubin, 1998; Hebey, 1996) implies

$$\|\phi^k\|_{L^6(\Gamma)}(t)\leq C\|\phi^k\|_{H^1(\Gamma)}(t)\leq C,\ t\in[0,T]\quad\text{for } n\leq 3$$

and

$$\|\phi^k\|_{L^\infty(0,T;L^6(\Gamma))}\leq C. \tag{18}$$

Due to zero Neumann boundary condition, the smoothness of Γ, and Green's identity we have for some $\delta>0$

$$\|\nabla^\Gamma\phi^k\|_{L^2(\Gamma)}^2\leq\|\phi^k\|_{L^2(\Gamma)}\|\Delta^\Gamma\phi^k\|_{L^2(\Gamma)}\leq\delta\|\Delta^\Gamma\phi^k\|_{L^2(\Gamma)}^2+\frac{1}{4\delta}\|\phi^k\|_{L^2(\Gamma)}. \tag{19}$$

Additionally, the regularity theory for the Laplace equation with zero Neumann boundary condition, defined on a smooth Riemannian manifold (Taylor, 1996, p. 344), implies the estimate

$$\|(\nabla^\Gamma)^2\phi^k\|_{L^2(\Gamma)}\leq C(\|\Delta^\Gamma\phi^k\|_{L^2(\Gamma)}+\|\phi^k\|_{L^2(\Gamma)}). \tag{20}$$

We consider now $v=\phi^k$ as a test function in (8) and integrate it with respect to time

$$\begin{aligned}
&\int_0^\tau\int_\Gamma\left(\frac{1}{2}\partial_t|\phi^k|^2+L_\phi\tilde{\sigma}\xi^2|\Delta^\Gamma\phi^k|^2+L_\phi\tilde{\sigma}|\phi^k|^2|\nabla^\Gamma\phi^k|^2\right)d\omega\,dt\\
&=\int_0^\tau\int_\Gamma L_\phi\Big(2\kappa'(\phi^k)(H-H_0(\phi^k))H_0'(\phi^k)\\
&\quad-\frac{1}{2}\kappa''(\phi^k)(H-H_0(\phi^k))^2-\kappa_G''(\phi^k)K+\tilde{\sigma}\\
&\quad+\kappa(\phi^k)((H-H_0(\phi^k))H_0''(\phi^k)-(H_0'(\phi^k))^2)\Big)|\nabla^\Gamma\phi^k|^2\,d\omega\,dt\\
&\quad+\int_0^\tau\int_\Gamma L_\phi(\kappa(\phi^k)H_0'(\phi^k)\nabla^\Gamma H-\kappa'(\phi^k)(H-H_0(\phi^k))\nabla^\Gamma H\\
&\quad-\kappa_G'(\phi^k)\nabla^\Gamma K)\nabla^\Gamma\phi^k\,d\omega\,dt.
\end{aligned} \tag{21}$$

Using the assumptions on f, κ, H_0 and κ_G, on the right hand side we obtain the terms of the form

$$\begin{aligned}
I_1&=\int_0^\tau\int_\Gamma(|\phi^k|+|\phi^k|^2+C)|\nabla^\Gamma\phi^k|^2\\
&\quad+(|\phi^k|+|\phi^k|^3+C)|\nabla^\Gamma\phi^k|\,d\omega\,dt,
\end{aligned}$$

that can be estimated by

$$\begin{aligned}
I_1&\leq C\int_0^\tau\int_\Gamma|\nabla^\Gamma\phi^k|^2\,d\omega\,dt+C\int_0^\tau\int_\Gamma(|\phi^k|^2+|\phi^k|^6)\,d\omega\,dt\\
&\quad+C\int_0^\tau\left(\int_\Gamma(|\phi^k|^3+|\phi^k|^6)\,d\omega\right)^{1/3}\left(\int_\Gamma|\nabla^\Gamma\phi^k|^3\,d\omega\right)^{2/3}dt+C\\
&\leq C\int_0^\tau\left(\int_\Gamma|\Delta^\Gamma\phi^k|^2\,d\omega\right)^{1/2}\left(\int_\Gamma|\phi^k|^6\,d\omega\right)^{1/6}\\
&\quad\times\left(\int_\Gamma(|\phi^k|^3+|\phi^k|^6)\,d\omega\right)^{1/3}dt\\
&\quad+C_{\delta_1}\int_0^\tau\int_\Gamma(|\phi^k|^6+|\phi^k|^3+|\phi^k|^2)\,d\omega\,dt\\
&\quad+\delta_1\int_0^\tau\int_\Gamma|\Delta^\Gamma\phi^k|^2\,d\omega\,dt+C\\
&\leq C_\delta\sup_{(0,T)}\|\phi^k\|_{L^6(\Gamma)}^6+\delta\int_0^\tau\int_\Gamma|\Delta^\Gamma\phi^k|^2\,d\omega\,dt+C,
\end{aligned} \tag{22}$$

where $\delta_1=L_\phi\tilde{\sigma}\xi^2/4$ and $\delta=L_\phi\tilde{\sigma}\xi^2/2$. Here, we have used the estimate (20) and the Gagliardo–Nirenberg inequality (Aubin, 1998, p. 93), given in the general form by

$$\|(\nabla^\Gamma)^j v\|_{L^p(\Gamma)}\leq C\|(\nabla^\Gamma)^m v\|_{L^r(\Gamma)}^\alpha\|v\|_{L^q(\Gamma)}^{1-\alpha}+C\|v\|_{L^q(\Gamma)}, \tag{23}$$

for $v\in L^q(\Gamma)$ and $(\nabla^\Gamma)^m v\in L^r(\Gamma)$, where $(j/m)\leq\alpha\leq 1$, $1/p=j/n+\alpha(1/r-m/n)+(1-\alpha)1/q$. In our situation, due to the estimate (20) and the continuous embedding $L^6(\Gamma)\subset L^2(\Gamma)$ for compact $\overline{\Gamma}$ (Hebey, 1999, p. 33), the used Gagliardo–Nirenberg inequality reads

$$\|\nabla^\Gamma\phi^k\|_{L^3(\Gamma)}\leq C\|\Delta^\Gamma\phi^k\|_{L^2(\Gamma)}^{1/2}\|\phi^k\|_{L^6(\Gamma)}^{1/2}+C\|\phi^k\|_{L^6(\Gamma)}\quad\text{for } n\leq 3.$$

Applying the estimates (18) and (22) in Eq. (21) implies

$$\begin{aligned}
&\int_0^\tau\int_\Gamma\left(\frac{1}{2}\partial_t|\phi^k|^2+L_\phi\tilde{\sigma}\xi^2|\Delta^\Gamma\phi^k|^2+\tilde{\sigma}|\phi^k|^2|\nabla^\Gamma\phi^k|^2\right)d\omega\,dt\\
&\quad\leq\int_0^\tau\int_\Gamma(\delta|\Delta^\Gamma\phi^k|^2+C_\delta)\,d\omega\,dt.
\end{aligned}$$

Then, integrating the first term with respect to time and using the regularity of the initial data we obtain the estimate

$$\|\phi^k\|_{L^\infty(0,T;L^2(\Gamma))}+\|\Delta^\Gamma\phi^k\|_{L^2(0,T;L^2(\Gamma))}\leq C.$$

To show the estimate for $(\Delta^\Gamma)^2\phi^k$ we choose $v=(\Delta^\Gamma)^2\phi^k$ as a test function in (8). As a basis of W_k we can consider the eigenfunctions of $(\Delta^\Gamma)^2$ with zero Neumann boundary conditions. Then, due to smoothness of Γ, it holds that $\phi^k\in C^\infty(\overline{\Gamma})$ (Taylor, 1996, p. 345, 379). Integration by parts and the boundary conditions (6) imply

$$\begin{aligned}
&\int_0^\tau\int_\Gamma\left(\frac{1}{2}\partial_t|\Delta^\Gamma\phi^k|^2+L_\phi\tilde{\sigma}\xi^2|(\Delta^\Gamma)^2\phi^k|^2\right)d\omega\,dt\\
&\quad=\int_0^\tau\int_\Gamma L_\phi\Delta^\Gamma R(\phi^k,H,K)(\Delta^\Gamma)^2\phi^k\,d\omega\,dt.
\end{aligned} \tag{24}$$

Due to zero-flux boundary conditions and regularity theory for elliptic operator of forth order (Taylor, 1996, p. 345, 379), we have

that $\|(\nabla^\Gamma)^4\phi^k\|_{L^2(\Gamma)} \le C(\|(\Delta^\Gamma)^2\phi^k\|_{L^2(\Gamma)} + \|\phi^k\|_{L^2(\Gamma)})$. Then, using the Gagliardo–Nirenberg inequality (23) we obtain the following estimates:

$$\begin{aligned}
\text{for } n=3: \quad & \|v\|_{L^{12}(\Gamma)} \le C\|(\Delta^\Gamma)^2 v\|_{L^2(\Gamma)}^{1/12}\|v\|_{L^6(\Gamma)}^{11/12} + C\|v\|_{L^6(\Gamma)},\\
& \|\nabla^\Gamma v\|_{L^6(\Gamma)} \le C\|(\Delta^\Gamma)^2 v\|_{L^2(\Gamma)}^{1/3}\|v\|_{L^6(\Gamma)}^{2/3} + C\|v\|_{L^6(\Gamma)},\\
& \|\Delta^\Gamma v\|_{L^3(\Gamma)} \le C\|(\Delta^\Gamma)^2 v\|_{L^2(\Gamma)}^{1/2}\|\nabla^\Gamma v\|_{L^2(\Gamma)}^{1/2} + C\|v\|_{H^1(\Gamma)},\\
\text{for } n=2: \quad & \|v\|_{L^{12}(\Gamma)} \le C\|(\Delta^\Gamma)^2 v\|_{L^2(\Gamma)}^{1/20}\|v\|_{L^6(\Gamma)}^{19/20} + C\|v\|_{L^6(\Gamma)},\\
& \|\nabla^\Gamma v\|_{L^6(\Gamma)} \le C\|(\Delta^\Gamma)^2 v\|_{L^2(\Gamma)}^{2/9}\|\nabla^\Gamma v\|_{L^2(\Gamma)}^{7/9} + C\|v\|_{H^1(\Gamma)},\\
& \|\Delta^\Gamma v\|_{L^3(\Gamma)} \le C\|(\Delta^\Gamma)^2 v\|_{L^2(\Gamma)}^{4/9}\|\nabla^\Gamma v\|_{L^2(\Gamma)}^{5/9} + C\|v\|_{H^1(\Gamma)}.
\end{aligned} \tag{25}$$

Now, to estimate the right hand side of (24) we have to consider terms of the form

$$I_2 = \int_0^\tau \int_\Gamma [(|\phi^k| + |\phi^k|^2 + C)|\nabla^\Gamma \phi^k| + (|\phi^k| + |\phi^k|^3)]|(\Delta^\Gamma)^2\phi^k|\, d\omega\, dt,$$

$$I_3 = \int_0^\tau \int_\Gamma (|\phi^k| + |\phi^k|^2 + C)(|\nabla^\Gamma \phi^k|^2 + |\Delta^\Gamma \phi^k|)|(\Delta^\Gamma)^2\phi^k|\, d\omega\, dt.$$

Using $\|\phi^k\|_{L^\infty(0,T;L^6(\Gamma))} \le C$, as well as $\|\nabla^\Gamma \phi^k\|_{L^\infty(0,T;L^2(\Gamma))} \le C$, and the correspondent estimates in (25) we can estimate the integrals I_2 and I_3 by

$$\begin{aligned}
I_2 &\le C_\delta \int_0^\tau \left(\int_\Gamma (|\phi^k|^6 + |\phi^k|^{12})\, d\omega\right)^{2/3} \|\nabla^\Gamma \phi^k\|_{L^6(\Gamma)}^2\, dt\\
&\quad + \delta \int_0^\tau \int_\Gamma |(\Delta^\Gamma)^2\phi^k|^2\, d\omega\, dt + C_\delta \int_0^\tau \int_\Gamma (|\phi^k|^2 + |\phi^k|^6)\, d\omega\, dt\\
&\le C_\delta \int_0^\tau \|(\Delta^\Gamma)^2\phi^k\|_{L^2(\Gamma)}\, dt + \delta \int_0^\tau \int_\Gamma |(\Delta^\Gamma)^2\phi^k|^2\, d\omega\, dt + C\\
&\le \delta \int_0^\tau \int_\Gamma |(\Delta^\Gamma)^2\phi^k|^2\, d\omega\, dt + C
\end{aligned}$$

and

$$\begin{aligned}
I_3 &\le C_\delta \int_0^\tau \left(\int_\Gamma (|\phi^k|^6 + |\phi^k|^{12} + C)\, d\omega\right)^{1/3}\\
&\quad \times (\|\Delta^\Gamma \phi^k\|_{L^3(\Gamma)}^2 + \|\nabla^\Gamma \phi^k\|_{L^6(\Gamma)}^4)\, dt\\
&\quad + \delta \int_0^\tau \int_\Gamma |(\Delta^\Gamma)^2\phi^k|^2\, d\omega\, dt \le \delta \int_0^\tau \int_\Gamma |(\Delta^\Gamma)^2\phi^k|^2\, d\omega\, dt\\
&\quad + C_\delta \int_0^\tau (\|(\Delta^\Gamma)^2\phi^k\|_{L^2(\Gamma)}^{1/3} + C)(\|(\Delta^\Gamma)^2\phi^k\|_{L^2(\Gamma)} + \|(\Delta^\Gamma)^2\phi^k\|_{L^2(\Gamma)}^{4/3} + C)\, dt\\
&\le \delta \int_0^\tau \int_\Gamma |(\Delta^\Gamma)^2\phi^k|^2\, d\omega\, dt + C_\delta.
\end{aligned}$$

Then, from (24), choosing $\delta = L_\phi \tilde\sigma \xi^2/4$, applying the integration by parts in the first term and the regularity assumption on the initial data, it follows

$$\int_\Gamma |\Delta^\Gamma \phi^k(\tau,x)|^2\, d\omega + \int_0^\tau \int_\Gamma |(\Delta^\Gamma)^2\phi^k(t,x)|^2\, d\omega\, dt \le C \quad \text{for all } \tau \in [0,T].$$

This estimate and Sobolev embedding theorem (Aubin, 1998; Hebey, 1999) imply

$$\|\phi^k\|_{L^\infty((0,T)\times\Gamma)} \le C, \quad \|\nabla^\Gamma \phi^k\|_{L^2(0,T;L^\infty(\Gamma))} \le C \quad \text{for } \dim(\Gamma) \le 3. \tag{26}$$

We choose now $v = \partial_t \phi^k$ as a test function in (8) and obtain after integration by parts and using the boundary conditions (6)

$$\begin{aligned}
&\int_0^\tau \int_\Gamma \left(|\partial_t \phi^k|^2 + \frac{L_\phi \tilde\sigma \xi^2}{2}\partial_t |\Delta^\Gamma \phi^k|^2\right) d\omega\, dt\\
&\quad = -\int_0^\tau \int_\Gamma L_\phi \nabla^\Gamma R(\phi^k, H, K)\nabla^\Gamma \phi_t^k\, d\omega\, dt\\
&\quad = \int_0^\tau \int_\Gamma L_\phi \Delta^\Gamma R(\phi^k, H, K)\phi_t^k\, d\omega\, dt.
\end{aligned}$$

The structure of f, assumptions on κ, H_0, κ_G, boundedness of ϕ^k in $(0,T)\times\Gamma$, Young inequality and the estimates (25) imply

$$\begin{aligned}
&\int_0^\tau \int_\Gamma \left[|\partial_t \phi^k|^2 + \frac{L_\phi \tilde\sigma}{2}(\xi^2 \partial_t |\Delta^\Gamma \phi^k|^2 + \partial_t(|\phi^k||\nabla^\Gamma \phi^k|)^2)\right] d\omega\, dt\\
&\quad \le C \int_0^\tau \int_\Gamma (|\nabla^\Gamma \phi^k|^2 + |\nabla^\Gamma \phi^k| + |\Delta^\Gamma \phi^k| + 1)\partial_t \phi^k\, d\omega\, dt\\
&\quad \le C_\delta \int_0^\tau \int_\Gamma (|(\Delta^\Gamma)^2\phi^k|^2 + |\nabla^\Gamma \phi^k|^2 + |\Delta^\Gamma \phi^k|^2 + 1)\, d\omega\, dt\\
&\qquad + \delta \int_0^\tau \int_\Gamma |\partial_t \phi^k|^2\, d\omega\, dt.
\end{aligned}$$

Then, by integrating with respect to t in the second and third terms and using the estimates for $\nabla^\Gamma \phi^k$ and $\Delta^\Gamma \phi^k$, as well as the regularity of the initial data, it follows

$$\int_0^T \int_\Gamma |\partial_t \phi^k|^2\, d\omega\, dt + \sup_{(0,T)} \int_\Gamma |\Delta^\Gamma \phi^k|^2\, d\omega \le C.$$

Passing to the limes as $k \to \infty$, using the weak convergence of a subsequence of $\{\phi^k\}$ to the solution of (4)–(6) and the lower semicontinuity of norms, yield the estimates (16) for ϕ. □

Proof of Theorem 3 Uniqueness. Here, we show the detailed estimates for the last integral in the equality (9). First we write the considered integral in the explicit form

$$\begin{aligned}
&\int_0^T \int_\Gamma \nabla^\Gamma (R(\phi_1) - R(\phi_2))\nabla^\Gamma(\phi_1 - \phi_2)\, d\omega\, dt\\
&\quad = \int_0^T \int_\Gamma \Big[\frac{1}{2}(\kappa''(\phi_1) - \kappa''(\phi_2))\nabla^\Gamma \phi_1 (H - H_0(\phi_1))^2\\
&\qquad + \frac{1}{2}\kappa''(\phi_2)(\nabla^\Gamma \phi_1 (H - H_0(\phi_1))^2 - \nabla^\Gamma \phi_2 (H - H_0(\phi_2))^2)\\
&\qquad + (\kappa'(\phi_1) - \kappa'(\phi_2))\Big(\nabla^\Gamma \phi_1 (H - H_0(\phi_1))H_0'(\phi_1) + \frac{1}{2}\nabla^\Gamma (H - H_0(\phi_1))^2\Big)\\
&\qquad + \kappa'(\phi_2)((\nabla^\Gamma \phi_1 (H - H_0(\phi_1))H_0'(\phi_1) - \nabla^\Gamma \phi_2 (H - H_0(\phi_2))H_0'(\phi_2)))\\
&\qquad + \frac{1}{2}\kappa'(\phi_2)\nabla^\Gamma ((H_0(\phi_1) - H_0(\phi_2))(H_0(\phi_1) + H_0(\phi_2) - 2H))\\
&\qquad + (\kappa(\phi_1) - \kappa(\phi_2))\nabla^\Gamma ((H - H_0(\phi_1))H_0'(\phi_1))\\
&\qquad + \kappa(\phi_2)\nabla^\Gamma ((H - H_0(\phi_1))(H_0'(\phi_1) - H_0'(\phi_2))\\
&\qquad + (H_0(\phi_1) - H_0(\phi_2))H_0'(\phi_2)) + (\kappa_G''(\phi_1) - \kappa_G''(\phi_2))\nabla^\Gamma \phi_2 K\\
&\qquad + \kappa_G''(\phi_2)(\nabla^\Gamma \phi_1 - \nabla^\Gamma \phi_2)K + (\kappa_G'(\phi_1) - \kappa_G'(\phi_2))\nabla^\Gamma K\\
&\qquad + f''(\phi_1)(\nabla^\Gamma \phi_1 - \nabla^\Gamma \phi_2) + (f''(\phi_1) - f''(\phi_2))\nabla^\Gamma \phi_2\Big]\nabla^\Gamma(\phi_1 - \phi_2)\, d\omega\, dt.
\end{aligned}$$

The last two terms can be rewritten as

$$\begin{aligned}
&\int_0^T \int_\Gamma (f''(\phi_1)\nabla^\Gamma(\phi_1 - \phi_2) + (f''(\phi_1) - f''(\phi_2))\nabla^\Gamma \phi_2)\nabla^\Gamma(\phi_1 - \phi_2)\, d\omega\, dt\\
&\quad = \frac{9}{8}\int_0^T \int_\Gamma ((3\phi_1^2 - 1)|\nabla^\Gamma(\phi_1 - \phi_2)|^2\\
&\qquad + 3(\phi_1^2 - \phi_2^2)\nabla^\Gamma \phi_2 \nabla^\Gamma(\phi_1 - \phi_2))\, d\omega\, dt.
\end{aligned}$$

From the assumptions on κ, H_0, κ_G it follows that κ, κ', κ'', κ_G', κ_G'', H_0, H_0', H_0'' are locally Lipschitz-continuous. Thus, the boundedness of ϕ_1 and ϕ_2 implies the estimate

$$\begin{aligned}
&\left|L_\phi \int_0^\tau \int_\Gamma \nabla^\Gamma (R(\phi_1) - R(\phi_2))\nabla^\Gamma(\phi_1 - \phi_2)\, d\omega\, dt\right|\\
&\quad \le C \int_0^\tau \int_\Gamma (|\phi_1 - \phi_2|(|\nabla^\Gamma \phi_1| + |\nabla^\Gamma \phi_2|)|\nabla^\Gamma(\phi_1 - \phi_2)|\\
&\qquad + |\nabla^\Gamma(\phi_1 - \phi_2)|^2)\, d\omega\, dt.
\end{aligned}$$

Applying Young inequality, the estimate (19) and the last estimate in (16) we obtain

$$\begin{aligned}
&\int_0^\tau \int_\Gamma |\phi_1-\phi_2|(|\nabla^\Gamma \phi_1|+|\nabla^\Gamma \phi_2|)|\nabla^\Gamma(\phi_1-\phi_2)|\, d\omega\, dt\\
&\quad \le \tilde{\delta}_1 \sup_{(0,\tau)} \int_\Gamma |\phi_1-\phi_2|^2\, d\omega \int_0^\tau \left(\sup_\Gamma |\nabla^\Gamma \phi_1|^2+\sup_\Gamma |\nabla^\Gamma \phi_2|^2\right) dt\\
&\qquad +\delta_2 \int_0^\tau \int_\Gamma |\Delta^\Gamma(\phi_1-\phi_2)|^2\, d\omega\, dt + C_{\delta_2} \int_0^\tau \int_\Gamma |\phi_1-\phi_2|^2\, d\omega\, dt\\
&\quad \le \delta_1 \sup_{(0,\tau)} \int_\Gamma |\phi_1-\phi_2|^2\, d\omega + \int_0^\tau \int_\Gamma (\delta_2 |\Delta^\Gamma(\phi_1-\phi_2)|^2\\
&\qquad + C_{\delta_2}|\phi_1-\phi_2|^2)\, d\omega\, dt,
\end{aligned}$$

where $0<\delta_1\le \frac{1}{4}$ and $0<\delta_2\le L_\phi \tilde{\sigma}\xi^2/2$. □

Appendix B

In terms of a local parametrization $\vec{X}: U\subset\mathbb{R}^n\to\Gamma$ of a smooth Riemannian manifold Γ the basis vectors of the tangential space are given by $\partial_{u_i}\vec{X}$ (using a shorter notation $\partial_i\vec{X}$), where $i=1,\dots,n$ and $u=(u_1,\dots,u_n)\in U$. Then the tensor $(g_{ij})_{i,j=1}^n$, with $g_{ij}=\partial_i\vec{X}\cdot\partial_j\vec{X}$, defines the first fundamental form or a local representation of the Riemannian metric on Γ and $(g^{ij})_{i,j}$ is the inverse of the first fundamental form. The second fundamental form $(b_{ij})_{i,j}$ is given by $b_{ij}=-\partial_i\vec{X}\cdot\partial_j\vec{n}$, where $\vec{n}$ is the unit normal vector on Γ.

In local coordinates the volume element (surface measure) is given by $d\omega=\sqrt{g}\,du_1\cdots du_n$, where $g=\det(g_{ij})_{i,j}$; the surface gradient is defined as $\nabla^\Gamma f=\sum_{i,j}g^{ij}\partial_j f\partial_i\vec{X}$; for each $\vec{a}=\sum_i a_i\partial_i\vec{X}$ the surface divergence is equal to $\nabla^\Gamma\cdot\vec{a}=g^{-1/2}\sum_i\partial_i(g^{1/2}a_i)$, hence the surface Laplacian is $\Delta^\Gamma f=\nabla^\Gamma\cdot\nabla^\Gamma f=g^{-1/2}\sum_{i,j}\partial_i(g^{1/2}g^{ij}\partial_j f)$. The mean curvature is equal to $H=\mathrm{trace}(b_i^j)$, where $b_i^j=\sum_k g^{kj}b_{ik}$, and the Gaussian curvature is given by $K=\det(b_i^j)$.

Adopting this notations we can rewrite Eq. (3) in local coordinates as follows:

$$\begin{aligned}
\partial_t\phi = L_\phi g^{-1/2}\sum_{i,j=1}^n \partial_i\Big(g^{1/2}g^{ij}\partial_j\Big(\frac{1}{2}\kappa'(\phi)(H-H_0(\phi))^2-\kappa(\phi)(H-H_0(\phi))H_0'(\phi)\\
+\kappa_G'(\phi)K-\tilde{\sigma}\xi^2 g^{-1/2}\sum_{i,j=1}^n\partial_i(g^{1/2}g^{ij}\partial_j\phi)+\tilde{\sigma}f'(\phi)\Big)\Big).
\end{aligned}$$

References

Alberts, B., Bray, D., Lewis, J., 2006. Molecular Biology of the Cell. Garland Publishing, Inc.

Allain, J.M., Amar, M.B., 2006. Budding and fission of a multiphase vesicle. Eur. Phys. J. E Soft Matter 20 (4), 409–420.

Aubin, T., 1998. Some Nonlinear Problems in Riemannian Geometry. Springer, Berlin, Heidelberg.

Barrett, J., Garcke, H., Nürnberg, R., 2008. Parametric approximation of Willmore flow and related geometric evolution equations. SIAM J. Sci. Comp. 31, 225–253.

Baumgart, T., Das, S., Webb, W.W., Jenkins, J.T., 2005. Membrane elasticity in giant vesicles with fluid phase coexistence. Biophys. J. 89 (2), 1067–1080.

Baumgart, T., Hess, S.T., Webb, W.W., 2003. Imaging coexisting fluid domains in biomembrane models coupling curvature and line tension. Nature 425 (6960), 821–824.

Becker, R., Braack, M., Dunne, T., Meidner, D., Richter, T., Vexler, B., 2012. Gascoigne 3d—a finite element toolbox, ⟨http://www.gascoigne.uni-hd.de⟩.

Bonifacino, J.S., Lippincott-Schwartz, J., 2003. Coat proteins: shaping membrane transport. Nat. Rev. Mol. Cell Biol. 4 (5), 409–414.

Bozic, B., Kralj-Iglic, V., Svetina, S., 2006. Coupling between vesicle shape and lateral distribution of mobile membrane inclusions. Phys. Rev. E Stat. Nonlin. Soft Matter Phys. 73 (4 Part 1), 041915.

Brannigan, G., Brown, F.L.H., 2005. Composition dependence of bilayer elasticity. J. Chem. Phys. 122 (7), 074905.

Brannigan, G., Brown, F.L.H., 2007. Contributions of Gaussian curvature and nonconstant lipid volume to protein deformation of lipid bilayers. Biophys. J. 92 (3), 864–876.

Brezzi, F., Fortin, M., 1991. Mixed and Hybrid Finite Element Methods. New York.

Cahn, J., Hilliard, J., 1958. Free energy of a nonuniform system: interfacial free energy. J. Chem. Phys. 28 (2), 258–267.

Chen, C.M., 1999. Theory for the bending anisotropy of lipid membranes and tubule formation. Phys. Rev. E Stat. Phys. Plasmas Fluids Relat. Interdiscip. Topics 59 (5 Part B), 6192–6195.

Ciarlet, O., 1997. Mathematical Elasticity: Theory of Plates, vol II, Studies in Mathematics and its Applications. North Holland, Amsterdam.

Cooke, I.R., Deserno, M., 2006. Coupling between lipid shape and membrane curvature. Biophys. J. 91 (2), 487–495.

Das, S., Jenkins, J., Baumgart, T., 2009. Neck geometry and shape transitions in vesicles with co-existing fluid phases: role of Gaussian curvature stiffness vs. spontaneous curvature. Europhys. Lett. 86, 1–6.

Derganc, J., 2007. Curvature-driven lateral segregation of membrane constituents in Golgi cisternae. Phys. Biol. 4 (4), 317–324.

Elliott, C., French, D., Milner, F., 1989. A second order splitting method for the Cahn–Hilliard equation. Numer. Math. 54, 575–590.

Elliott, C., Garcke, H., 1996. On the Cahn–Hilliard equation with degenerate mobility. SIAM J. Math. Anal. 27, 404–423.

Elliott, C., Songmu, Z., 1986. On the Cahn–Hilliard equation. Arch. Rat. Mech. Anal. 96, 339–357.

Elliott, C.M., Stinner, B., 2010. Modeling and computation of two phase geometric biomembranes using surface finite elements. J. Comp. Phys. 229 (18), 6598–6612.

Evans, L., 1998. Partial Differential Equations. AMS, Providence, RI.

Gennis, R., 1989. Biomembranes: Molecular Structure and Function. Springer-Verlag, New York.

Hebey, E., 1996. Sobolev Spaces on Riemannian Manifolds. Springer, Berlin, Heidelberg.

Hebey, E., 1999. Nonlinear Analysis on Manifolds: Sobolev Spaces and Inequalities. Courant Lecture Notes, New York.

Heinrich, M., Tian, A., Esposito, C., Baumgart, T., 2010. Dynamic sorting of lipids and proteins in membrane tubes with a moving phase boundary. Proc. Natl. Acad. Sci. USA 107 (16), 7208–7213.

Helfrich, W., 1973. Elastic properties of lipid bilayers: theory and possible experiments. Z. Naturforsch. (C) 28 (11), 693–703.

Illya, G., Lipowsky, R., Shillcock, J.C., 2006. Two-component membrane material properties and domain formation from dissipative particle dynamics. J. Chem. Phys. 125 (11), 114710.

Imparato, A., Shillcock, J., Lipowsky, R., 2005. Shape fluctuations and elastic properties of two-component bilayer membranes. Europhys. Lett. 69, 650–656.

Jakobsen, A.F., 2005. Constant-pressure and constant-surface tension simulations in dissipative particle dynamics. J. Chem. Phys. 122 (12), 124901.

Jiang, Y., Lookman, T., Saxena, A., 2000. Phase separation and shape deformation of two-phase membranes. Phys. Rev. E Stat. Phys. Plasmas Fluids Relat. Interdiscip. Topics 61 (1), R57–R60.

Kamal, M., Mills, D., Grzybek, M., Howard, J., 2009. Measurement of the membrane curvature preference of phospholipids reveals only weak coupling between lipid shape and leaflet curvature. Proc. Natl. Acad. Sci. USA 106 (52), 22245–22250.

Kranenburg, M., Venturoli, M., Smit, B., 2003. Molecular simulations of mesoscopic bilayer phases. Phys. Rev. E Stat. Nonlin. Soft Matter Phys. 67 (6 Part 1), 060901.

Kwak, D., 2007. The Sharp-interface Limit of the Cahn–Hilliard System with Elasticity. Dissertation.

Laradji, M., Kumar, P.B.S., 2005. Domain growth, budding, and fission in phase-separating self-assembled fluid bilayers. J. Chem. Phys. 123 (22), 224902.

Laradji, M., Kumar, P.S., 2004. Dynamics of domain growth in self-assembled fluid vesicles. Phys. Rev. Lett. 93, 198105.

Lee, A.G., 2005. Lipid sorting: lipids do it on their own. Curr. Biol. 15 (11), R421–R423.

Leibler, S., 1986. Curvature instability in membranes. J. Phys. 47, 507–516.

Li, J., Zhang, H., Tang, P., Qiu, F., Yang, Y., 2006. A discrete, space variation model for studying the kinetics of shape deformation of vesicles coupled with phase separation. Macromol. Theor. Simul. 15, 432–439.

Li, L., Lin, M., Qui, F., 2005. Lateral separation and budding of giant vesicles. Acta Chim. Sin. 63 (14), 1375–1378.

Liang, Q., Ma, Y.Q., 2009. Curvature-induced lateral organization in mixed lipid bilayers supported on a corrugated substrate. J. Phys. Chem. B 113 (23), 8049–8055.

Lions, J.-L., 1969. Quelques Methodes de Resolution des Problemes aux Limites Non Lineaires. Dunod.

Lowengrub, J.S., Rätz, A., Voigt, A., 2009. Phase-field modeling of the dynamics of multicomponent vesicles: spinodal decomposition, coarsening, budding, and fission. Phys. Rev. E Stat. Nonlin. Soft Matter Phys. 79 (3 Part 1), 031926.

Mercker, M., Richter, T., Hartmann, D., 2011. Sorting mechanisms and communication in phase-separating coupled monolayers. J. Phys. Chem. B 115, 11739–11745.

Mullins, C., 2005. Molecular Biology Intelligence Unit: The Biogenesis of Cellular Organelles. Plenum Publishers, New York.

Nikunen, P., Karttunen, M., Vattulainen, I., 2003. How would you integrate the equations of motion in dissipative particle dynamics simulations? Comp. Phys. Commun. 153, 407–421.
Parthasarathy, R., Yu, C., Groves, J., 2006. Curvature-modulated phase separation in lipid bilayer membranes. Langmuir 22 (11), 5095–5099.
Pencer, J., Jackson, A., Kucerka, N., Nieh, M.P., Katsaras, J., 2008. The influence of curvature on membrane domains. Eur. Biophys. J. 37 (5), 665–671.
Ramaswamy, S., Toner, J., Prost, J., 2000. Nonequilibrium fluctuations, traveling waves, and instabilities in active membranes. Phys. Rev. Lett. 84 (15), 3494–3497.
Rawicz, W., Olbrich, K.C., McIntosh, T., Needham, D., Evans, E., 2000. Effect of chain length and unsaturation on elasticity of lipid bilayers. Biophys. J. 79 (1), 328–339.
Risselada, H.J., Marrink, S.J., 2009. Curvature effects on lipid packing and dynamics in liposomes revealed by coarse grained molecular dynamics simulations. Phys. Chem. Chem. Phys. 11 (12), 2056–2067.
Roux, A., Cuvelier, D., Nassoy, P., Prost, J., Bassereau, P., Goud, B., 2005. Role of curvature and phase transition in lipid sorting and fission of membrane tubules. EMBO J. 24 (8), 1537–1545.
Rózycki, B., Weikl, T.R., Lipowsky, R., 2008. Stable patterns of membrane domains at corrugated substrates. Phys. Rev. Lett. 100 (9), 098103.
Schmidt, U., Guigas, G., Weiss, M., 2008. Cluster formation of transmembrane proteins due to hydrophobic mismatching. Phys. Rev. Lett. 101 (12), 128104.
Schwarz, U., Gompper, G., 2002. Bicontinuous surfaces in self-assembling amphiphilic systems. Lecture Notes in Physics, vol. 600; 2002.
Seifert, U., 1993. Curvature-induced lateral phase segregation in two-component vesicles. Phys. Rev. Lett. 70 (9), 1335–1338.
Seifert, U., 1997. Configurations of fluid membranes and vesicles. Adv. Phys. Lett. 46, 13–137.
Semrau, S., Idema, T., Holtzer, L., Schmidt, T., Storm, C., 2008. Accurate determination of elastic parameters for multicomponent membranes. Phys. Rev. Lett. 100 (8), 088101.
Siegel, D.P., 2008. The Gaussian curvature elastic energy of intermediates in membrane fusion. Biophys. J. 95 (11), 5200–5215.
Siegel, D.P., Kozlov, M.M., 2004. The Gaussian curvature elastic modulus of *n*-monomethylated dioleoylphosphatidylethanolamine: relevance to membrane fusion and lipid phase behavior. Biophys. J. 87 (1), 366–374.
Singer, S.J., Nicolson, G.L., 1972. The fluid mosaic model of the structure of cell membranes. Science 175 (23), 720–731.
Sugar, I.P., Mizuno, N.K., Momsen, M.M., Brockman, H.L., 2001. Lipid lateral organization in fluid interfaces controls the rate of colipase association. Biophys. J. 81 (6), 3387–3397.
Szleifer, I., Kramer, D., Ben-Shaul, A., Roux, D., Gelbart, M., 1988. Curvature elasticity of pure and mixed surfactant films. Phys. Rev. Lett. 60 (19), 1966–1969.
Taniguchi, T., 1996. Shape deformation and phase separation dynamics of two-component vesicles. Phys. Rev. Lett. 76 (23), 4444–4447.
Taylor, M., 1996. Partial Differential Equations I, III. Springer.
Tian, A., Baumgart, T., 2009. Sorting of lipids and proteins in membrane curvature gradients. Biophys. J. 96 (7), 2676–2688.
Wang, X., Du, Q., 2008. Modelling and simulations of multi-component lipid membranes and open membranes via diffuse interface approaches. J. Math. Biol. 56 (3), 347–371.
Yamamoto, A.S.H., 2003. Budding and fission dynamics of two-component vesicles. J. Chem. Phys. 118 (17), 7937–7943.
Yamamoto, S., Maruyama, Y., Hyodo, S., 2002. Dissipative particle dynamics study of spontaneous vesicle formation. J. Chem. Phys. 116, 5842.
Yin, Y., Lv, C., 2008. Equilibrium theory and geometrical constraint equation for two-component lipid bilayer vesicles. J. Biol. Phys. 34 (6), 591–610.
Yoon, T.Y., Jeong, C., Lee, S.W., Kim, J.H., Choi, M.C., Kim, S.J., Kim, M.W., Lee, S.D., 2006. Topographic control of lipid-raft reconstitution in model membranes. Nat. Mater. 5 (4), 281–285.
Yoshigaki, T., 2007. Theoretically predicted effects of Gaussian curvature on lateral diffusion of membrane molecules. Phys. Rev. E Stat. Nonlin. Soft Matter Phys. 75 (4 Part 1), 041901.